Theory of singlet oxygen emission photosensitized by porphyrins

ARTICLE *in* PROCEEDINGS OF SPIE - THE INTERNATIONAL SOCIETY FOR OPTICAL ENGINEERING · OCTOBER 2006

Impact Factor: 0.2 · DOI: 10.1117/12.689617

2 AUTHORS:

Boris Minaev
Черкаський національний унів...
327 PUBLICATIONS **3,194** CITATIONS
SEE PROFILE

G. I. Kobzev
Orenburg State University
19 PUBLICATIONS **80** CITATIONS
SEE PROFILE

Available online at www.sciencedirect.com
SCIENCE DIRECT®
Spectrochimica Acta Part A 59 (2003) 3387–3410
SPECTROCHIMICA ACTA PART A
www.elsevier.com/locate/saa

Response calculations of electronic and vibrational transitions in molecular oxygen induced by interaction with noble gases

Boris F. Minaev [a,b,*], G.I. Kobzev [c]

[a] Cherkassy Engineering and Technological Institute, 257006 Cherkassy, Ukraine
[b] Laboratory of Theoretical Chemistry, The Royal Institute of Technology, SCFAB Roslagstullsbacken 15, Stockholm 10691, Sweden
[c] Department of Chemistry, Orenbourg University, 460352 Orenbourg, Russia

Received 6 January 2003; received in revised form 31 March 2003; accepted 2 April 2003

Abstract

The Einstein coefficient for the singlet oxygen emission $a^1\Delta_g \rightarrow X^3\Sigma_g^-$ at $\lambda = 1270$ nm and $b^1\Sigma_g^+ \rightarrow X^3\Sigma_g^-$ emission at $\lambda = 750$ nm were calculated by quadratic response (QR) multiconfiguration self-consisted field (MCSCF) method for a number of collision complexes O_2+M, where M = He, Ne, Ar. Interaction with He clusters was studied in order to simulate cooperative effect of the environment on the oxygen emission. Calculations of the dipole transition moment for the Noxon band, $b^1\Sigma_g^+ - a^1\Delta_g$, by linear response (LR) MCSCF method were also performed for a number of collision complexes. Spin-orbit coupling (SOC) between the $b^1\Sigma_g^+$ and $X^3\Sigma_g^-$ ($M_S = 0$) states does not change much upon collisions, thus the $a-X$ transition borrows intensity mostly from the collision-induced Noxon band $b-a$. The $a-X$ intensity borrowing from the Schumann–Runge transition is negligible. The calculations show that the $b-a$ and $a-X$ transition probabilities are enhanced approximately by 10^5 and 10^3 times by O_2+M collisions. An order of magnitude differences occur for both transitions for noble gases with large difference in polarizability. A strong cooperative effect is obtained when few He atoms perturb the oxygen molecule. Depending on mutual orientation of the partners it can be a complete quenching of the $a \rightarrow X$ emission or strong non-additive enhancement. Collision-induced infrared vibrational transitions in a number of molecular oxygen excited states were studied and shown to be state selective.

Keywords: Collision complexes; O_2+He; O_2+Ne; O_2+Ar; Spin-orbit coupling; MCSCF response calculations

1. Introduction

Intermolecular interactions between dioxygen and noble gases induce a number of interesting optical phenomena [1–4]. The oxygen molecule possesses a triplet ground state, $X^3\Sigma_g^-$, and two low-lying singlet excited states, $a^1\Delta_g$ and $b^1\Sigma_g^+$, which lie only 0.98 and 1.63 eV, respectively, above the ground term; thus the singlet–triplet (S–T) transitions in the visible and near infrared regions are the most prominent features in atmospheric spectroscopy in spite of their forbidden

* Corresponding author.
E-mail address: boris@theochem.kth.se (B.F. Minaev).

1386-1425/03/$ - see front matter © 2003 Elsevier B.V. All rights reserved.
doi:10.1016/S1386-1425(03)00165-3

character [5]. The oxygen molecule has quite specific spin-orbit coupling (SOC) and the S–T transition probabilities [6,7]. The influence of intermolecular interactions on the radiative S–T transitions in normal diamagnetic molecules (for example, in aromatics) in the absence of external heavy atoms or paramagnetic species is not very important [8,9]. In sharp contrast to this, one finds that the radiative decay of singlet molecular oxygen, $a^1\Delta_g \rightarrow X^3\Sigma_g^-$, is very sensitive to collisions in gas phase [1–3] and to weak intermolecular interactions in solid noble gas matrices [10–12] and in liquid solvents [13–22,18,23]. The basic understanding of this sensitivity is essential from the point of view of the singlet oxygen importance in photophysics (I_2 laser pumping [11], quenching of dyes, sensors [9], etc.), in photochemistry [14,24], in biochemistry and medicine [25–28,23]. The singlet oxygen $O_2(a^1\Delta_g)$ is easily populated by photo-sensitization, i.e. by the T–S energy transfer from triplet excited dyes [9,13]. The $O_2(a^1\Delta_g)$ species is more reactive than the ground state oxygen [14]. Photo-sensitized oxidation by singlet oxygen can play an important role in oxidative damage of live matter because natural cells constituents such as porphyrins or flavins can act as sensitizers of the singlet oxygen $O_2(a^1\Delta_g)$.

This is the reason for increased interest in theoretical interpretation of the intermolecular interaction effect on radiative lifetime of the singlet oxygen $a^1\Delta_g$ and $b^1\Sigma_g^+$ states during last few years [18,29,21,30–37]. The theory [38,39] proposed 15 years ago is grounded on the prediction of great enhancement of the $b^1\Sigma_g^+ \rightarrow a^1\Delta_g$ transition probability by intermolecular interaction. According to the theory of S–T transitions in free O_2 molecule [7,6] a strong intra-molecular SOC effect mixes the $b^1\Sigma_g^+$ and $X^3\Sigma_g^-$ ($M_S = 0$) states in O_2 molecule; this leads to the $a^1\Delta_g \rightarrow X^3\Sigma_g^-$ band intensity borrowing from the $b^1\Sigma_g^+ \rightarrow a^1\Delta_g$ transition [38,39]. Calculations of some models of collision complexes [38,40–42] indicate that other sources of intensity borrowing (for example, from the Schumann–Runge transition) are not so much important like the above mechanism. In this paper direct ab initio calculation of the $a^1\Delta_g \rightarrow X^3\Sigma_g^-$ transition probability by multireference self-consistent field (MCSCF) quadratic response (QR) method [43] for few models of collision complexes O_2+M (where M is a noble gas atom) are presented for the first time.

Geometry optimization of the O_2+M complexes in a number of excited states of oxygen moiety has permitted us to calculate vibrational frequencies and the infrared absorption intensity induced by collision. These quantities are also discussed here, since they correlate with the electronic transitions enhancement. A weak collision-induced IR absorption of O_2 molecule near 6.4 μm (1563 cm^{-1}) is well known [4]. We have studied the dependence of this collision-induced IR intensity on polarizability of collider and on geometry of collision. The collision induced IR intensity is studied for a number of states of O_2 molecule.

2. Method of calculations

Multiconfiguration self-consisted field (MCSCF) method in a complete active space (CAS) [44] is a general basis for the present approach. The singlet–singlet (S–S) transitions are calculated by linear response (LR) method [45]; the poles of the response function give the excitation energies and the residues at the excitation frequency give the S–S transition moments to the corresponding excited states. The $b^1\Sigma_g^+ \rightarrow a^1\Delta_g$ transition intensity of oxygen moiety in collision complexes is calculated here by this method. The S–T transitions are forbidden in the non-relativistic approximation; SOC mixes the spin multiplicity and gives rise to a non-vanishing transition dipole moment which can be calculated as the residue of a QR function at the excitation frequency of the S–T transition [43]. MCSCF QR calculations of collision complexes O_2+M provide the $a^1\Delta_g \rightarrow X^3\Sigma_g^-$ transition probability through collision-induced electric dipole moment of the first S–T transition in the system. For example, a collision complexes between the O_2 molecule and the He atom has the triplet ground state wave function:

$$^3\Psi[X^3\Sigma_g^-(O_2),\ ^1S(He)] = \mathscr{A}(1\sigma_g)^2(1\sigma_u)^2(2\sigma_g)^2(1s,He)^2(2\sigma_u)^2(3\sigma_g)^2(\pi_u)^4 \times (\pi_{z,g})^1(\pi_{x,g})^1, \quad (1)$$

where $\mathscr{A}$ indicates the proper anti-symmetrization product; $\pi_{z,g}$ and $\pi_{x,g}$ are two quasi-degenerate π_g orbitals mostly localized on the oxygen moiety. At a triangle (or T-shaped) geometry (Fig. 1a) the triplet ground state has the $^3B_1$ symmetry in the C_{2v} point group since the open shell orbitals, $\pi_{z,g}$ and $\pi_{x,g}$, belong to the b_2 and a_2 irreducible representations, respectively. At large intermolecular distances ($R \geq 3$ Å) the energies of the MOs are not changed much from those of the separated molecules and their wave functions are similar to the orbitals of a single molecule. So the nature of each MO is well determined as belonging to one particular molecular partner of collision. This also follows from the Mulliken population analysis of the MCSCF wave functions. By these reasons it is easy to assign each state in the complex as being locally excited in one or in both molecules. The $a^1\Delta_g$ state is doubly degenerate in free O_2 molecule. One of its component has the same orbital structure like the triplet counterpart, Eq. (1). The orbital symmetry of both states is B_1. The second component of the $a^1\Delta_g$ state in the complex:

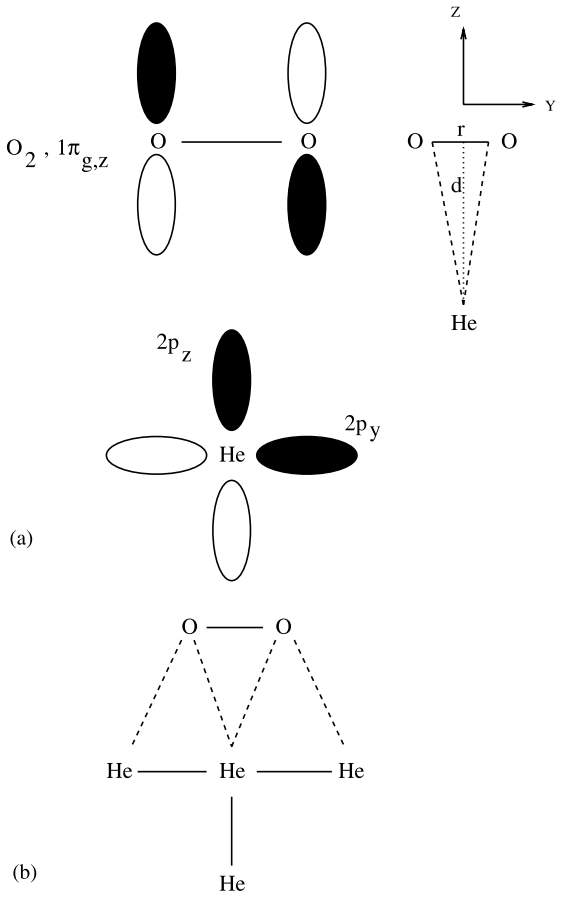

Fig. 1. Structural and orbital overlap model of the collision complexes between oxygen molecule and a rare gas atom (a); a model of the O_2 interaction with the He cluster (b).

$$^1\Psi_2[a^1\Delta_g(O_2),\ ^1S(He)] = \mathscr{A}(1\sigma_g)^2(1\sigma_u)^2(2\sigma_g)^2(1s,He)^2(2\sigma_u)^2(3\sigma_g)^2(\pi_u)^4 \times \frac{1}{\sqrt{2}}[(\pi_{z,g})^2 - (\pi_{x,g})^2] \quad (2)$$

which will be denoted in the following as "a" state, has the $^1A_1$ symmetry.

There is also the third singlet state

$$^1\Psi[b^1\Sigma_g^+(O_2),\ ^1S(He)] = \mathscr{A}(1\sigma_g)^2(1\sigma_u)^2(2\sigma_g)^2(1s,He)^2(2\sigma_u)^2(3\sigma_g)^2(\pi_u)^4 \times \frac{1}{\sqrt{2}}[(\pi_{z,g})^2 + (\pi_{x,g})^2] \quad (3)$$

The singlet states, Eqs. (2) and (3), are totally symmetrical. MCSCF calculations were performed for the lowest state of the $^1A_1$ symmetry Eq. (2); then the LR method has been applied for the ground singlet state MCSCF wave function and the a–b transition frequency and probability have been calculated.

The singlet–triplet (S–T) transition probability may be described in terms of QR function that corresponds to the molecular electronic shell response to SOC which is treated as a perturbation [43]. A big advantage of the QR method is that the general sum-over-states expression of perturbation theory for the S–T transition dipole moment [8] is replaced by solution of sets of linear equations, which may be solved by iterative technique. For details of the QR method we refer to [43]. The SOC operator is implemented here in the complete Breit–Pauli form [43]. The S–T transition electric dipole moment

$$D^{\xi}(T^{\gamma}) = \left\langle S| \sum_i e\xi_i | T^{\gamma} \right\rangle \quad (4)$$

determines light polarization along ξ axis, when light is emitted to the T^{γ} spin sublevel. Since the complexes have low symmetry, the Cartesian triplet components T^{γ} ($\gamma = x, y, z$) are employed [43]

$$T^x = \frac{T^{-1} - T^1}{\sqrt{2}}, \qquad T^y = i\frac{T^{-1} + T^1}{\sqrt{2}}, \qquad T^z = T^0 \quad (5)$$

These are eigenfunctions of the zero-field-splitting (ZFS) Hamiltonian [9]; since the triplet state open shell is localized on the oxygen moiety the ZFS pattern is very similar to the pure oxygen ZFS parameters, $D = 3.95\ \mathrm{cm}^{-1}$, $E = 0$ [7,38].

In this work calculations of spectral properties of collision complexes were performed by MCSCF QR method with account of the 6-311G* basis set [46] and the correlation consistent basis of Dunning et al. augmented by polarization functions, aug-cc-pvDZ, aug-cc-pvQZ [47]; for the complex containing Ar atom the 6-31G basis set [48] is used for comparison. This basis is also employed for qualitative configuration interaction studies of a large number of collision-induced transitions.

The choice of axes for the complexes is given in Fig. 1. In the MCSCF calculations the inner shells orbitals and the $2\sigma_g$–MO on oxygen moiety are inactive; the CAS includes all other occupied orbitals presented in Eq. (2). The orbitals of rare gas atom are not included in CAS MCSCF calculations. The $3\sigma_u$ and the two $2\pi_u$ MOs on oxygen are added to all CAS used in this work. The CAS described above is called CAS-I. Some extensions of this CAS are used for comparison and discussed in the text.

Geometry optimization of the O_2+He complex at the MCSCF level has been carried out for the six states, $B^3\Sigma_u^-$, $A'^3\Delta_u$, $b^1\Sigma_g^+$, $a^1\Delta_g$, $a'^1\Delta_g$, $X^3\Sigma_g^-$ using the C_{2v} symmetry constraint. All calculations for O_2+He complex presented in Tables 1–5, 10–12 are done with the aug-cc-pvDZ basis set. Other complexes are calculated with this and other basis sets as it is described in the text. The calculations were performed with the GAMESS [49,50] and with the DALTON [51] program packages.

3. Results and discussion

The theory of the "singlet oxygen" radiative lifetime at nonzero pressure and in condense media has been discussed before [38–40,52]. Although the old theory of transition intensities in free O_2 molecule [6,53] and the theory of their enhancement in collision complexes [38,39] were based on configuration interaction calculations of semiempirical (MINDO/3) type, its conceptual validity seems to be confirmed, and the main ideas do not depend crucially on the approximations involved. Ab initio calculations [54,35,55,56] have thus supported predictions of the old theory [53,57,38] for the b–a, b–X and a–X transition probabilities in free O_2 molecule, including the internuclear distance dependence of the magnetic dipole moment and its connection with g-factor. Recent ab initio studies [58,59,34,33] gave additional support to the collision-induced intensity borrowing mechanisms [39]. But direct ab initio calculation of the a–X transition probability enhancement by collision have not been reported yet. This is the aim of the present work.

The high symmetry of free O_2 molecule ($D_{\infty h}$) implies sharp selection rules for oxygen spectroscopy. All transitions between the low-lying family of states $X^3\Sigma_g^-$, $a^1\Delta_g$ and $b^1\Sigma_g^+$ are strictly forbidden: they are doubly forbidden by orbital selection rules and the singlet–triplet a–X and b–X transitions have additional prohibition by the spin selection rule. Nevertheless the singlet–triplet b–X transition is the most intensive. The near-infrared band ($a^1\Delta_g \rightarrow X^3\Sigma_g^-$ transition, 1270 nm) and the infrared Noxon band ($b^1\Sigma_g^+ \rightarrow a^1\Delta_g$ transition, $\lambda = 1908$ nm) are extremely weak. The Einstein coefficient for spontaneous emission are equal 0.0002 [60] and 0.0014 s^{-1} [61], respectively. The atmospheric red emission ($b^1\Sigma_g^+ \rightarrow X^3\Sigma_g^-$ transition in the free O_2 molecule at $\lambda = 760$ nm) is much stronger [5,62–64]. Measured Einstein coefficient A_{b-X} is equal 0.087 s^{-1} [62,63]; the red atmospheric oxygen emission is among the bright-

Table 1
Results of the MCSCF LR calculations for different triplet and singlet states of the O_2+He complex at the intermolecular distance d = 3 Å

Ψ_n	ΔE (eV)	$\langle b^1\Sigma_g^+ \lvert H_{so} \rvert \Psi_n \rangle$ (cm^{-1})	$\langle b^1\Sigma_g^+ \lvert D \rvert \Psi_n \rangle$ (ea_0)	E_n (a.u.)
$X^3\Sigma_g^-(^3B_1)$	−1.764	160.59	–	−152.67400
$a^1\Delta_g(^1A_1)$	−0.639	–	0.0031	−152.63266
$a'^1\Delta_g'(^1B_1)$	−0.639	0	0.0025	−152.63266
$b^1\Sigma_g^+(^1A_1)$	0	–	–	−152.60918
$c^1\Sigma_y^-(^1A_2)$	4.374	–	0	−152.44744
$A'^3\Delta_u(^3B_2)$	4.408	−0.028	–	−152.44718
$A^3\Sigma_u^+(^3B_2)$	4.572	−0.063	–	−152.44117
$1^3\Pi_g(^3B_2)$	6.429	−67.77	–	−152.37293
$1^3\Pi_g(^3A_2)$	6.428	−67.74	–	−152.37293
$B^3\Sigma_u^-(^3A_2)$	7.242	−0.296	–	−152.34304
$1^1\Pi_g(^1B_2)$	8.018	–	0.080	−152.30718
$2^3\Pi_g(^3B_2)$	8.353	−9.642	–	−152.30220
$2^3\Pi_g(^3A_2)$	8.350	10.256	–	−152.30226
$1^3\Pi_u(^3B_1)$	7.504	−0.029	–	−152.33342
$1^3\Pi_u(^3A_1)$	7.504	–	–	−152.33339
$1^1\Pi_u(^1A_1)$	7.670	–	0.233	−152.32730
$1^1\Pi_u(^1B_1)$	7.667	–	0.228	−152.32741
$2^3\Pi_u(^3B_1)$	11.000	−0.220	–	−152.20494
$2^3\Pi_u(^3A_1)$	11.000	0	–	−152.20494

He is being in the ground state ^1S. The $b^1\Sigma_g^+$ state is the MCSCF reference state. RAS2 is constructed as the CAS-I, RAS3 includes $4\sigma_g$ and $2\pi_g$–MO's; 79 428 determinants.

est features of the air night-glow. Both $b-a$ and $a-X$ transitions are magnetic dipole in nature [5,53,65]; the great difference in their probabilities is explained by an additional spin-current contribution to the magnetic dipole transition moment of the former transition [6,35,52–54,65].

Table 2
QR calculations of the $a^1\Delta_g \rightarrow X^3\Sigma_g^-$ transition intensity, induced by the O_2+He collision

d (Å)	$D^z_{a-X}(T^y)$ (ea_0)	ΔE_{a-X} (a.u.)	τ_R (s)	A^z_{a-X} (s^{-1})	A^y_{a-X} (s^{-1})	E ($a^1\Delta_g$) (a.u.)	α_{zz}	α_{yy}
2.6	0.000028	0.053862	393	2.54×10^{-3}	2.67×10^{-7}	−152.582001	8.307	14.1398
2.8	0.000022	0.053893	637.3	1.57×10^{-3}	7.35×10^{-8}	−152.582609	8.6544	14.1901
3.0	0.000017	0.053909	1014	0.98×10^{-3}	7.2×10^{-8}	−152.582886	8.6290	14.2311
3.2	0.000014	0.053917	1619	0.61×10^{-3}	5.5×10^{-8}	−152.582997	8.5985	14.2646
3.4	0.000011	0.053922	2572	3.89×10^{-4}	4.56×10^{-8}	−152.583031	8.5689	14.2906
3.6	0.000009	0.053926	3907	0.26×10^{-3}	4.1×10^{-8}	−152.583037	8.5428	14.3103
3.8	0.000007	0.053928	5942	1.68×10^{-4}	3.96×10^{-8}	−152.583034	8.5205	14.3251
4.2	0.000005	0.053924	13 097	0.76×10^{-4}	3.68×10^{-8}	−152.583027	8.4857	14.3453
5.0	0.000003	0.053929	41 038	0.24×10^{-4}	2.05×10^{-8}	−152.583020	8.4449	14.3686
6.0	0.000001	0.053928	1.99×10^{5}	5.01×10^{-6}	0.67×10^{-8}	−152.583019	8.4239	14.3843
8.0	0.000001	0.053928	1.71×10^{5}	5.83×10^{-6}	0.74×10^{-8}	−152.583019	8.4094	14.3975
10.0	0.000001	0.053928	8.6×10^{5}	1.16×10^{-6}	1.29×10^{-10}	−152.583019	8.4043	14.4022
20.0	0.000000	0.053928	5.0×10^{6}	0.21×10^{-6}	0.52×10^{-12}	−152.583019	8.3995	14.4066

D is electric dipole $a-X$ transition moment, obtained at different intermolecular distances (d) for the C_{2v} geometry of the T-shaped collision (Fig. 1a), r_{O-O} = 1.207 Å. CAS-I (2996 determinants). τ_R is a radiative lifetime of the $a^1\Delta_g(^1A_1)$ state, α_{zz} is a dynamic polarizability (a_0^3) along perpendicular axis at a frequency of the $a-X$ transition.

Table 3
LR calculations of the $b^1\Sigma_g^+ - a^1\Delta_g$ transition and the SOC matrix element (in cm^{-1}) between the $b-X$ states, obtained at different intermolecular distances for the C_{2v} geometry of the O_2+He collision, $r_{O-O} = 1.207$ Å, D_{a-b} is electric dipole $a-b$ transition moment d is intermolecular distance

d (Å)	$\langle b^1\Sigma_g^+ \lvert H_{so}^y \rvert X^3\Sigma_g^- \rangle$	D_{a-b} (ea_0)	ΔE_{a-b} (a.u.)	E ($b^1\Sigma_g^+$) (a.u.)
2.6	161.560	0.005976	0.018953	−152.555560
2.8	161.7	0.004754	0.019026	−152.555881
3.0	161.752	0.003788	0.019062	−152.556406
3.2	161.777	0.002984	0.019080	−152.556512
3.4	161.79	0.002368	0.019090	−152.556511
3.6	161.795	0.001897	0.019097	−152.556547
3.8	161.802	0.001539	0.019101	−152.556543
4.2	161.804	0.001056	0.019107	−152.556535
5.0	161.807	0.000580	0.019109	−152.556528
6.0	161.811	0.000291	0.019109	−152.556526
8.0	161.812	0.000095	0.019109	−152.556526
10.0	161.811	0.000040	0.019109	−152.556526
20.0	161.811	0.000003	0.019109	−152.556526
40.0	161.811	1.6×10^{-7}	0.019109	−152.556526

Let us denote the non-relativistic 0-order MCSCF wave functions by $\Psi(n\Sigma\Lambda\Omega)$ and the SOC-perturbed wave functions by Φ_n, where n is a spectroscopic term notation. Thus we have:

$$\Phi_b = \Psi(b^1\Sigma_g^+) + C_{b,x}\Psi(X^3\Sigma_{g,0}^-) \tag{6}$$

and

$$\Phi_{X,0} = \Psi(X^3\Sigma_{g,0}^-) - C_{b,X}^*\Psi(b^1\Sigma_g^+), \tag{7}$$

where

$$C_{b,X} = \frac{\langle\Psi(X^3\Sigma_{g,0}^-)|H_{so}|\Psi(b^1\Sigma_g^+)\rangle}{E_b - E_X}. \tag{8}$$

Here $\Psi(X^3\Sigma_{g,0}^-)$ corresponds to the $\Omega = 0$, where Ω is the total electronic angular momentum quantum number $\Omega = \Lambda + \Sigma$. In an effective one-electron approximation the SOC matrix element in the numerator of Eq. (8) is equal to $-i\zeta_O$, where $\zeta_O = 153\ cm^{-1}$ is the SOC constant for the $O(^3P)$ atom. Ab initio calculations [54,66,35] gave $-176i\ cm^{-1}$. Accounting for the experimental energy difference in the denominator of Eq. (8),

Table 4
QR calculations of the $b^1\Sigma_g^+ \rightarrow X^3\Sigma_g^-$ transition intensity, induced by the O_2+He collision. D (ea_0) is electric dipole $b-X$ transition moment, obtained at different intermolecular distances for the C_{2v} geometry of collision; d is intermolecular distance, τ_R is a radiative lifetime of the $b^1\Sigma_g^+(2^1A_1)$ state, A^z is the Einstein coefficient for spontaneous emission polarized along z axis

d (Å)	$D_{b-X}^z(T^y)$	$D_{b-X}^y(T^z)$	ΔE_{b-X} (a.u.)	τ_R (s)	A_{b-X}^z (s^{-1})	A_{b-X}^y (s^{-1})	$E(b^1\Sigma_g^+)$ (a.u.)
2.8	0.000007	0.000013	0.071417	568.3	1.40×10^{-3}	3.61×10^{-4}	−152.556142
3.0	0.000006	0.000009	0.071433	1077	0.67×10^{-3}	2.51×10^{-4}	−152.556407
3.2	0.000003	0.000007	0.071440	2226	0.37×10^{-3}	7.39×10^{-5}	−152.556512
3.4	0.000002	0.000005	0.071444	4087	2.01×10^{-4}	3.56×10^{-5}	−152.556543
3.6	0.000001	0.000004	0.071446	7769	0.12×10^{-3}	1.09×10^{-5}	−152.556547
3.8	0.000001	0.000003	0.071448	13 691	0.71×10^{-4}	3.06×10^{-6}	−152.556543
4.2	0.000000	0.000002	0.071451	35 122	0.28×10^{-4}	2.03×10^{-7}	−152.556535
5.0	0.000000	0.000000	0.071452	1.50×10^5	0.60×10^{-5}	5.79×10^{-8}	−152.556528
6.0	0.000000	0.000000	0.071452	6.03×10^5	1.63×10^{-6}	1.11×10^{-8}	−152.556527
8.0	0.000000	0.000000	0.071452	5.87×10^6	0.17×10^{-6}	0.80×10^{-9}	−152.556527

Table 5
QR calculations of the $a^1\Delta_g \rightarrow X^3\Sigma_g^-$ transition intensity, induced by the O_2+Ne collision

d (Å)	$D^z_{a-X}(T^y)$	$D^y_{a-X}(T^z)$	ΔE_{a-X} (a.u.)	τ_R (s)	A^z_{a-X} (s^{-1})	A^y_{a-X} (s^{-1})	E($a^1\Delta_g$) (a.u.)
2.8	0.000026	0.000001	0.053871	448.6	2.23×10^{-3}	0.12×10^{-5}	−278.222740
3.0	0.000021	0.000000	0.053897	671.5	1.49×10^{-3}	0.62×10^{-7}	−278.223321
3.2	0.000017	0.000000	0.053911	1080	0.92×10^{-3}	0.31×10^{-6}	−278.223554
3.4	0.000013	0.000000	0.053919	1636	0.61×10^{-3}	1.85×10^{-7}	−278.223649
3.6	0.000011	0.000000	0.053923	2361	0.42×10^{-3}	1.09×10^{-7}	−278.223686
3.8	0.000009	0.000000	0.053926	3381	0.30×10^{-3}	0.74×10^{-7}	−278.223695

D is electric dipole $a-X$ transition moment, obtained at different intermolecular distances (d) for the C_{2v} geometry of the T-shaped collision (Fig. 1a), d is intermolecular distance, τ_R is a radiative lifetime of the $a^1\Delta_g(1^1A_1)$ state, A^z is the Einstein coefficient for spontaneous emission polarized along z axis. CAS-I, aug-cc-pVDZ basis set.

13195 cm^{-1} [67], the admixture coefficient $C_{b,X}$ is equal to $-0.0134i$. This coefficient plays a crucial role for the explanation of the radiative properties of molecular oxygen in zero pressure gas phase and in solvents in the framework of the old theory [7,38–40]. The appreciable admixture of singlet $^1\Sigma_g^+$ character into the triplet $\Phi_{X,0}$ state, Eq. (7), affords the $a-X$,0 transition to borrow intensity from the $b-a$ Noxon band.

$$\langle\Phi_a|\hat{T}|\Phi_{X,0}\rangle = -C^*_{b,X}\langle\Psi(a^1\Delta_g)|\hat{T}|\Psi(b^1\Sigma_g^+)\rangle, \qquad (9)$$

In this general expression $\hat{T}$ is an arbitrary multipole in the expansion of the radiation field. In free O_2 molecule the $\hat{T}$ is a quadrupole ($\hat{Q}$). The $b-a$ transition has an electric-quadrupole moment, $Q_{b-a} = 1.005\ ea_0^2$ [57,54], which induces a corresponding $a-X$,0 transition quadrupole moment; $Q_{a-X,0} = -C_{b,X}{}^*Q_{b-a} = -i0.0135\ ea_0^2$. Electric-quadrupole contributions to the intensity of the $a-X$,0 transition is practically negligible; $A_{a-X,0} = 5\times10^{-7}\ s^{-1}$ [54,57]. In free O_2 molecule the $a-X$ emission band (1270 nm) consists practically only from magnetic radiation (transition $a-X$,1 to the $\Omega=1$ spin sublevel).

In dense gases, in rare gas matrices and in solvents the radiative properties of the $a^1\Delta_g$ singlet state of molecular oxygen are changed drastically. It was shown first by absorption measurements in gas phase [68] that the $a-X$ transition probability usually is enhanced by 10^3–10^4 times by collisions, while the $b-X$ transition intensity is only slightly changed in the absence of external heavy atom effect. The same trends have been observed in emission in gases [3,2], solid matrices [10,12] and in solvents [13,15,69,16,70–72,22,73,18]. The reason for such selective enhancement is not connected with the fact that the $b-X$ transition is already relatively strong inside free O_2 molecule and that the $a-X$ transition is 400 times weaker, but rather with peculiarity of the open shell $1\pi_g^2$ configuration response to electrostatic perturbations. The peculiar SOC mixing, Eq. (7), is also important. At the same time the "spin capacity" of the b, a and X states, i.e. the possibility to accept other multiplicities, does not changed much upon collision [38,42].

3.1. Qualitative analysis of the $b-a$ and $a-X$ transitions enhancement by collisions

Analysis of the response of the open $1\pi_g^2$ shell to the intermolecular perturbation in collision complexes between O_2 and H_2 molecules shows that the collision-induced electric-dipole moment ($\hat{D} = e\Sigma_i r_i$) of the $b-a$ transition is the important characteristic feature of such complexes [39]:

$$D_{b-a} = \langle{}^1\Psi[b^1\Sigma_g^+(O_2), X^1\Sigma_g^+(H_2)]|\hat{D}|^1\Psi_2 \times[a^1\Delta_g(O_2), X^1\Sigma_g^+(H_2)]\rangle = \frac{1}{2}(D_z - D_x), \qquad (10)$$

where wave functions $^1\Psi[b^1\Sigma_g^+]$ and $^1\Psi[a^1\Delta_g]$ are similar to wave functions given in Eqs. (2) and (3). Obviously, the ($1s$, He) orbital should be changed by the ($1\sigma_g$, H_2) molecular orbital. The D_z and D_x are expectation values of the electric dipole moment for the doubly occupied $\pi_{z,g}$ and $\pi_{x,g}$ orbitals, respectively [39]:

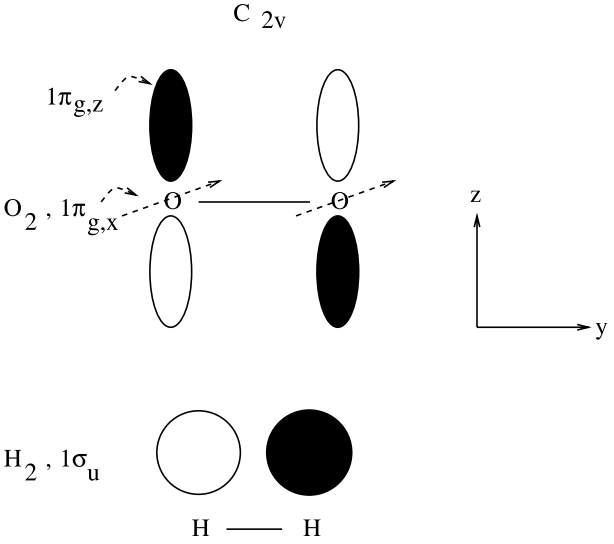

Fig. 2. Structural and orbital overlap model of the collision complexes between oxygen and hydrogen molecules.

$$D_z = 2\langle\psi(\pi_{z,g})|\hat{D}|\psi(\pi_{z,g})\rangle. \quad (11)$$

It is assumed that all MO's are the same in both states $b^1\Sigma_g^+$ and $a^1\Delta_g$. This is the case in a simple semiempirical MINDO/3 CI approximation [38,39]. In the collision complex (Fig. 2) the $\pi_{z,g}$–MO has an admixture of hydrogen 1s-orbitals:

$$\pi_{z,g} = 0.7[p_z(\mathrm{O}) - p_z(O')] + 0.01[1s(\mathrm{H}) - 1s(H')],$$

$$\pi_{x,g} = \frac{1}{\sqrt{2}}[p_x(\mathrm{O}) - p_x(O')] \quad (12)$$

In a minimal valence basis set there is no admixture of hydrogen 1s-orbitals to the $\pi_{x,g}$ orbital, since there is no overlap between oxygen p_x–AOs and 1s-orbitals of hydrogen; thus $D_y = 0$. Even small 1s-admixture to the $\pi_{z,g}$–MO produces an appreciable contribution to the D_x expectation value [39].

$$D_z = 4 \times 0.01\langle\phi(1s)|\hat{D}|\phi(1s)\rangle \simeq 0.04ez_H, \quad (13)$$

where z_H is a coordinate of H atom along z-axis; the origin of the coordinate system is on the middle of the O_2 molecule. In that case z_H is the intermolecular distance. Since the intermolecular distance is large ($\sim 5a_0$), the D_z integral is also comparatively large and is about 0.2 ea_0 [38,39]. From this simple picture it is easy to see that such a collision induces an appreciable ($D_{b-a} \sim 0.1\ ea_0$) electric dipole b–a transition moment [39]. (The electric dipole transition b–a' for the $^1B_1$ component of the $a^1\Delta_g$ state is still forbidden in such a simple model). At non-symmetrical collision both transitions b–a and b–a' are getting allowed but the total transition intensity is comparable with the previous one [38,34].

The admixture coefficient (0.01 in Eq. (12) is a result of the empty $1\sigma_u$–MO admixture to the ground state. It can be easily shown [38,34] that this admixture depends on polarizablity of hydrogen molecule: mixing with empty orbitals is equivalent to the mixing between the ground and excited states. In a simplest way this mixing occurs on the Hartree–Fock level, when intermolecular interaction is considered inside the collision complex, treated as a super-molecule. The collision induced electric dipole transition moment between $b^1\Sigma_g^+$ and $a^1\Delta_g$ states inside the oxygen moiety occurs at very long intermolecular distance [38], when other transitions induced by exchange and charge-transfer interactions still remain forbidden [39,58,34,74].

Similar result can be obtained for the O_2+He complex. The electric dipole transition moment between the $a^1\Delta_g$ state Eq. (2) and its "+" signed counterpart (state $b^1\Sigma_g^+$, Eq. (3)) is also equal to $\frac{1}{2}(D_z - D_x)$. The $\pi_{z,g}$–MO now contains an admixture of the $2p_y$–AO of He atom, while the $\pi_{x,g}$ orbital has no contribution from the $2p_x$–AO of helium in a minimal basis set (Fig. 1a). In this approximation the difference $D_z - D_x$ of the two collision-induced dipoles and the electric dipole transition moment D_{b-a} depend on the admixture of the $2p$(He) empty orbital, i.e. on the polarizability of the collider. Thus in a minimal basis set the $b^1\Sigma_g^+$–$a^1\Delta_g$ transition dipole moment in a good approximation is equal to:

$$D_{b-a} = \frac{1}{2}D_z = C_{\pi_{z,g}}^{\mathrm{He}(p_y)} \cdot z_{\mathrm{He}} \quad (14)$$

In a large basis set the $\pi_{x,g}$ orbital has a

contribution from the $3d_{2-}$ orbital of helium atom. Thus the difference of the orbital dipole moments $D_z - D_x$ induced in the collision complex O_2+He in a large basis set depends on the difference of polarizability (α) and of the second hyperpolarizability (γ) of the He atom; the former quantity determines the admixture of the $2p_y$–AO in an electric field of the O_2 quadrupole moment, the last quantity determines the admixture of the $3d_{2-}$ orbitals of helium in the field of the oxygen quadrupole. Since the electric dipole transition moment (Eq. (14)) depends on the difference $D_z - D_x$ of the two collision-induced dipoles it is easy to understand that polarizability of the collider and its higher-order hyperpolarizability are getting important. Geometry of collision and orbital overlap of two partners are also of crucial importance. The simple model (Fig. 1a), Eqs. (2), (3) and (10), illustrates qualitative idea of the $b-a$ transition enhancement in an obvious manner. The admixture coefficient for the $\pi_{z,g}$–MO in the O_2+H_2 complex is proportional to the overlap and to the polarizabilities of H_2 and O_2 molecules in the perpendicular direction. For N_2 partner the collision induced electric dipole $b-a$ transition moment (analogous to Eq. (10)) in O_2+N_2 complex depends on the difference of $\pi-\pi$ and $\sigma-\sigma$ overlaps and on the difference of polarizabilities in the perpendicular and in the parallel directions. In order to check predictions of the simple semiempirical theory [38,52] the closed shell rare gas atoms with different polarizability are used in this work for studies of the $b-a$ and $a-X$ transition probabilities.

It was predicted by CI calculations [58] that the $b-a$ radiation acquires the electric-dipole transition moment $D_{b-a} = 0.0114$ e Å for O_2+H_2 at the intermolecular distance $R = 2.8$ Å, which corresponds to $A_{b-a} = 140\ s^{-1}$ and to enhancement of the intensity of the Noxon band by 10^5 times. Because the Noxon transition, $b-a$, acquires an electric dipole character upon collisions, it contributes to the intensity of the $a-X$ radiation, see Eq. (9). The collisions induced electric dipole character ($\hat{D}$) of the $a-X$,0 band can be obtained by a simple substitution $\hat{T} = \hat{D}$ in Eq. (9):

$$\begin{aligned} D_{a-X,0} &= \langle \Phi(a^1\Delta_g)|\hat{D}|\Phi_{X,0}\rangle \\ &= \langle \Psi(a^1\Delta_g)|\hat{D}|\Psi(X^3\Sigma^-_{g,M_S=0}) \\ &\quad - C^*_{b,X}\Psi(b^1\Sigma^+_g)\rangle \\ &= -C^*_{b,X}\langle \Psi(a^1\Delta_g)|\hat{D}|\Psi(b^1\Sigma^+_g)\rangle \\ &= -C^*_{b,X}D_{a-b}. \end{aligned} \quad (15)$$

In the O_2+H_2 collision the induced electric dipole transition moment $\langle a^1\Delta_g|\hat{D}|b^1\Sigma^+_g\rangle$ is of the order 0.01 e Å [58], which corresponds to the $a-X$ transition moment equals 0.00013 Å and to the Einstein coefficient for the $a \to X$ spontaneous emission $A_{x-a} \simeq 0.2\ s^{-1}$. This means three orders of magnitude enhancement of the $a^1\Delta_g$ singlet oxygen emission probability in comparison with the collision-free zero pressure limit. This is the aim of the present work to check applicability of the simple theory, Eq. (15) for different collision complexes by direct MCSCF QR calculations of the collision induced $a-X$ transition dipole moment.

3.2. O_2+He collision

The MCSCF geometry optimization for the ground state van der Waals complex, O_2+He produces two minima, one corresponds to the T-shaped structure of the C_{2v} symmetry (Fig. 1a) with $d = 3.26$ Å; the second stable isomer has a linear structure with the nearest O–He distance equals about 4 Å. In this calculations the $2p-$CAS$+2\sigma_u+2\pi_u$ MO's have been used as a CAS (CAS-I). Results of the MCSCF geometry optimization in this CAS-I for a number of states in linear and T-shaped forms are presented in Tables 9 and 10, respectively. In CAS-I the linear form is slightly more stable (0.14 kJ mol^{-1}) than the T-shaped van der Waals complex. The opposite result has been obtained in larger active space which includes additionally the $4\sigma_g$ MO and $2\pi_g$ MO's; these MO's have been treated by restricted active space (RAS-3) with account of all single and double excitations from the CAS. The total number of determinants is 79428. Results of LR calculations of the T shaped O_2+He complexes in RAS-3 with the $b^1\Sigma^+_g$ term as a reference state are presented in Table 1.

The nearest O–He distance in linear structure (4 Å) is much longer than in the T-shaped structure (3.3 Å). We get a convergence of geometry optimization for larger number of states in linear structure (Table 9). A weakly bound $^5\Pi_g$ state of the van der Waals complex between two ground state oxygen atoms $O(^3P)+O(^3P)$ was predicted before [75]; we found its internuclear distance (3.25 Å) in O_2 system to be shorter than in more sophisticated MRCI calculation (3.8–4.2 Å) [75]. Vibrational frequency (ω) obtained in our MCSCF geometry optimization (58.8 cm^{-1}) is smaller than ω obtained in the most accurate MRCI calculation(105 cm^{-1}) [75]. Inspite a qualitative nature of our MCSCF results, we feel that the relative stability of different states in the O_2+He van der Waals complexes (Tables 9 and 10) reflects some realistic features. From this point of view it is interesting to note that the weakly bound three-bodies complex O···O···He in the $^5\Pi_g$ state is characterized by the most intensive infrared absorption; the anticipated 60–105 cm^{-1} vibrational IR transition of the $^5\Pi_g$ state of O_2 molecule is getting electric-dipole allowed upon weak intermolecular interaction with buffer gases.

The collision-induced IR absorption of O_2 near 6.4 μm (the ground state vibrational frequency $\omega = 1563$ cm^{-1}) is well known [4]. This fundamental band absorption participates in radiative process in the Earth's atmosphere. The O_2–O_2 and O_2–N_2 collisions in the air induce the weak IR absorption, which is seen when large optical paths are considered [4]. The collisions with noble gases also induce the infrared absorption of O_2; our MCSCF calculations of the collision-induced dipole moment derivatives show that infrared transitions intensity (IRI) strongly increases when we compare He, Ne and Ar colliders. In linear collisions IRI is higher than in "T"-shaped collisions; this is natural since the collision-induced dipole moment occurs along O–O axis. In the ground state of linear complex the dipole gradient in normal coordinate basis is equal -0.002235 Debye (Å) $(amu)^{-1/2}$, which corresponds to IRI = 0.0001 km mol^{-1}. (Values less than 0.001 km mol^{-1} are not shown in Table 9, amu is atomic mass unit). From the present calculations one can predict a correlation between the collision induced IR absorption of O_2 near 6.4 μm and the a–b and a–X transitions intensity. It is interesting to note that the collision-induced IR absorption in the singlet oxygen $O_2(a^1\Delta_g)$ molecule near 1500 cm^{-1} should has higher probability (Table 9).

The shift of vibrational frequency in low-lying states of all complexes is not large. For example, the vibrational frequencies in the X, a and b states of free O_2 molecule are equal (in the same CAS-I–D calculations) 1548.0, 1454.1 and 1370.3 cm^{-1}, respectively. Comparison with Table 9 indicates only small (3.7 cm^{-1}) shift in the $a^1\Delta_g$ state of linear complex. In the $A'^3\Delta_u$ state the calculated ω is 755.6 cm^{-1} for free O_2 molecule; the splitting of these states and shifts of their vibrational frequencies are quite substantial in "T"-shaped complex (Table 10). The strongly stabilized $^3B_2$ component of the $A'^3\Delta_u$ state in nonlinear O_2+He complex has also an enhancement of the IR absorption (Table 10).

Let us consider the electronic transitions enhancement. The collision induced a–b (and hence the a–X,0) transition is very sensitive to the active space. The use of the RASs was found nonrelaible in this respect. For example, inclusion of the $2\pi_g$–MO's in RAS-3 with account of doubly excited configurations from the following RAS-2 active space ($2p-CAS+2\sigma_u+2\pi_g$) leads to a qualitative change of the $a^1\Delta_g$ wave function of the $^1A_1$ symmetry (Eq. (2)); instead of mixture of two configurations (Eq. (2)) it becomes almost a closed shell wave function.

Such a transformation does not cost much energy, but it changes the a–b (and especially the a–X,0) transition moment and the SOC matrix element drastically. This produces a physically unreasonable enhancement of the a–X,0 transition moment. Since the enlargement of the active space is unstable in respect to such spontaneous change of the $a^1\Delta_g$ wave function of the $^1A_1$ symmetry, one should take care about the physically reasonable result of MRCI. Only these results are discussed in the present paper. Consideration of asymmetric collision complex geometry also leads to the spontaneous change of the $a^1\Delta_g$ wave function even in the framework of the same CAS. By this reason only C_{2v} geometry has been studied.

Two CASs are used in $He+O_2$ complexes. The small one includes $2\sigma_u$, $3\sigma_g$, $1-2\pi_u$, $1\pi_g$-orbitals; this is CAS-I which corresponds to 3996 determinants (ten electrons in nine orbitals). The largest one, CAS-II, includes additionally $4\sigma_g$ orbital and two $2\pi_g$ MO's, which corresponds to 156 832 determinants for the triplet states (10 electrons in 12 orbitals). Both CAS produce similar results for the $a-b$ transition moment in oxygen moiety, but the CAS-II produces better excited states energy. For example, at $d=5$ Å, the vertical $b-X$ and $b-a$ transitions energy are equal 1.85 and 0.85 eV in CAS-I; these quantities in CAS-II are 1.72 and 0.68 eV, respectively, in much better agreement with experimental data for O_2 molecule, 1.65 and 0.66 eV, respectively [67].

The basis set extension from the "aug-cc-pVDZ" to "aug-cc-pVTZ" does not influence much the results of the QR calculation for the $a-X$,0 transition moment: at $d=2.6$ Å it changed from 0.000028 ea_0 (CAS-I–D) to 0.000025 ea_0 (CAS-I–T); D and T refer to the corresponding basis set.

Since equilibrium geometries of different states differ, the equilibrium ground state r_{O-O} distance have been used for the $a\rightarrow X$ and $b\rightarrow X$ transition intensity. Scanning the intermolecular distance d (distance between the He atom and the center of the O–O bond in "T"-shaped complex) we found that the minimum on potential energy surface (PES) is shifted from 3.26 Å (Table 10) to 3.6 Å (Table 2). It means that the minimum on the PES is very shallow and could be easily shifted by small variation of the O–O bond length.

After the intermolecular distance $d=3$ Å is achieved, a very strong rise of the potential energy starts to grow (Tables 2 and 3), thus the point $d=3$ Å cab be considered as the shortest contact achieved in collisions. The points, where d equals 2.6 and 2.8 Å, only illustrate the trend in the collision induced moments.

It follows from Table 2 that only $D^z(T^y)$ component of the $a-X$,0 transition is enhanced in collisions. (The T^y spin sublevel corresponds to zero spin projection on the O_2 axis, y, Fig. 1). The z axis corresponds to the intermolecular direction (Fig. 1). Only z component of the $a-b$ transition dipole moment is induced during collision (Fig. 1b) as it follows from simple consideration (Eq. (14)). The $a-b$ transition dipole moment is really the largest one among all other collision induced dipole moments at long intermolecular distances (Tables 3 and 1). In Table 3 only the 1^1A_1 component of the double degenerate $a^1\Delta_g$ state is presented. The second component, 1^1B_1, has weaker intensity: the $a'-b$ transition moment at $d>3.4$ Å is an order of magnitude smaller (and the intensity is two order of magnitude weaker) for the $1^1B_1-2^1A_1$ transition. Thus the consideration of the second component is omitted in Table 3.

The calculated $D^y_{a-X}(T^z)$ component of the $a-X$,1 transition which borrows intensity from the collision induced $^3\Pi_g-X^3\Sigma_g^-$ and other similar transitions [38,42] is less than 10^{-7}, so it is not shown in Table 2. But the corresponding Einstein coefficient, A^y_{a-X}, is presented in this Table and indicates that the collision induced electric dipole $a-X$,1 emission is four order of magnitude weaker than the radiation induced by D^z component of the $a-X$,0 transition (Table 2). These results support the previous semiempirical estimation [38,42].

It is interesting to note that the simple $2p-$CAS ($3\sigma_{g,u}$, $1\pi_{g,u}$; only 61 determinants) produces reasonable results from the LR calculation; for example at $d=3.4$ Å one gets $E_a=-152.54146$ hartree, $D^z_{a-b}=0.0025$ ea_0, $E_{a-b}=0.898$ eV. But the QR results are not so good; the calculated D^z_{a-X} transition moment is underestimated at all distances.

Electronic structure of oxygen molecule does not change much upon collisions. The most important quantities for this study—the SOC matrix elements—are almost the same like in free oxygen molecule (Table 1). The collision induced SOC matrix elements $\langle b^1\Sigma_g^+|H_{so}|A^3\Sigma_u^-\rangle$ are negligible even at a very short contact, $d=3$ Å (Table 1). The largest SOC integral occurring upon collision, $\langle b^1\Sigma_g^+|H_{so}|B^3\Sigma_u^-\rangle$, does not exceed 0.3 cm^{-1}. It seems that the QR results strongly depend on the proper description of highly excited states; in small CASs, which do not include the $2\sigma_u$ and especially the $2\pi_{g,u}$–MOs, the main D^z_{a-X} contribution (Eq. (15)) is quenched by strongly overestimated intermolecular transitions.

In a simple consideration, Eq. (15), the $a-X$,0 transition in the collision complex borrows intensity from the collision induced $a-b$ transition, because of strong SOC, Eq. (8). From Table 3 one can see that the absolute value of the SOC integral in the numerator of the Eq. (8) does not change much upon collision; the change is negligible even at the equilibrium ($d_e = 3.6$ Å) distance. Similar results have been obtained before in semiempirical MINDO/3 CI approximation [38,40]. The assumption that the SOC mixing coefficient, Eq. (8), is not changed upon collisions have been used in many previous studies [58,59,33,34]. Account of only one contribution, Eq. (15), based on results of Table 3 reproduces the largest part of the calculated $D^z_{a-X}(T^y)$ transition moment by the QR MCSCF method with large active space (CAS-II); at the same time it is higher than the result of the QR method in CAS-I. Thus the prediction of the simple theory, Eq. (15), is in the middle between CAS-I and CAS-II QR MCSCF calculations, which include thousands terms in perturbation theory treatment. The He atom is a very weak perturber of the oxygen spectrum [2,3]. In CAS-I the calculated Einstein coefficient for spontaneous $a-X$ emission is about 10^{-3} s^{-1} at $d = 3.2$ Å (Table 2), which corresponds to the radiative lifetime of about 10^3 s. In CAS-II the calculated Einstein coefficient is equal 0.014 s^{-1} at $d = 3.2$ Å, which corresponds to the radiative lifetime 69 s. In CAS-II calculation the $a-b$ transition moment is only slightly increased ($D_{a-b} = 0.0031$ ea_0) in comparison with the CAS-I result (Table 2). Definitely, the increase of the active space leads to some additional states which contribute to increase of the $a-X$ intensity. This is not connected with the basis set superposition error, since the increase of the basis set to aug-cc-pVTZ and even to cc-pVQZ bases does not change much neither the $a-b$ nor the $a-X$ transition moments in LR and QR treatments at $d = 3.2$ Å with the CAS-I MCSCF $a^1\Delta_g$ reference state. It is difficult to observe an enhancement of the singlet oxygen emission [2,3]. Fink et al. [2] studied the collision-induced $b \rightarrow a$ oxygen emission on addition of foreign gases. Bimolecular rate constants for such emission have been measured from the ratio of the intensities of the discrete lines and the collision-induced continuum appearing under the discrete lines. They range from $\leq 10^{-21}$ cm^3 s^{-1} for He to 4.2×10^{-19} cm^3 s^{-1} for PCl_3 vapor. For Ne, Ar and Kr the bimolecular rate constants are equal 10^{-21}, 17×10^{-21} and 36×10^{-21} cm^3 s^{-1}, respectively [2]. Results for He are just on the border of sensitivity of the method and Ne produces slightly higher increase with pressure. Wildt et al. [3] studied the collision-induced $a \rightarrow X$ oxygen emission in the presence of Ar, Kr, Xe, N_2 and other gases. Narrow continua were found for the (0,0) band; for diamagnetic gases the continua distinctly narrower than for O_2 and NO and thus they are more difficult to measure. This is natural since the paramagnetic molecules induce the electric dipole $a \rightarrow X$ transition moment without spin-forbidden selection rule: direct CI calculations without SOC account reproduces the order of magnitude of the $a \rightarrow X$ band enhancement [38,37].

Measurements of the a state radiative lifetime (τ_a) in noble gas matrices [12] indicate that for Ne, Ar and Kr matrices τ_a is 146, 68 and 34 s, respectively. Our CAS-II QR calculations for He complex definitely overestimate the $a-X$ transition probability and underestimate the radiative lifetime ($\tau_a = 69$ s). CAS-I results probably give the lower limit for the $a-X$ transition moment.

Since the further increase of the active space leads to physically unreliable $a^1\Delta_g$ wave function in the O_2+He collision complex at any distances, we shall consider CAS-I calculations for comparison between He and Ne complexes with O_2.

3.3. O_2+Ne collision

Exactly the same CAS has been used for O_2+Ne complex, like for the O_2+He collision; Ne and He orbitals have not been included in CAS and only $2\sigma_u$, $3\sigma_g$, $1-2\pi_u$, $1\pi_g$-orbitals of the oxygen moiety constituted the CAS (CAS-I). All Ne occupied orbitals are lower in energy than the $2\sigma_u$–MO of oxygen. Results of the MCSCF CAS-I-D QR calculations of the $a-X$ transition intensity are presented in Table 5. Comparison with the similar calculations of the O_2+He complex (Table 2) indicates that Ne produces slightly more strong enhancement: at short intermolecular dis-

Table 6
QR calculations of the $a^1\Delta_g \rightarrow X^3\Sigma_g^-$ transition intensity, obtained with different basis sets for the C_{2v} geometry of the O_2+Ne collision, D (ea_0) is electric dipole $a-X$ transition moment, the intermolecular distance is 3.4 Å, τ_R is a radiative lifetime of the $a^1\Delta_g(1^1A_1)$ state, A^z is the Einstein coefficient for spontaneous emission polarized along z axis

Basis set	$D^z_{a-X}(T^y)$	$D^y_{a-X}(T^z)$	ΔE_{a-X} (a.u.)	τ_R (s)	A^z_{a-X} (s^{-1})	A^y_{a-X} (s^{-1})	E($a^1\Delta_g$) (a.u.)
6-311++G(2d,2p)	0.000010	0.000000	0.0554133	2931	0.34×10^{-3}	0.83×10^{-7}	−278.197042
6-311++G(3df,3pd)	0.000015	0.000000	0.054868	1199	0.84×10^{-3}	0.37×10^{-6}	−278.203054
cc-pVQZ	0.000012	0.000001	0.054999	1796	0.55×10^{-3}	0.63×10^{-6}	−278.316886
aug-cc-pVDZ	0.000013	0.000000	0.053919	1636	0.61×10^{-3}	1.85×10^{-7}	−278.223649

CAS-I (3996 determinants).

tances $d=2.8$–3.2 Å the D^z_{a-X} transition moment induced by Ne collision is about 15–18% higher than that induced by the O_2 collision with He atom.

Small non-zero D^y_{a-X} component occurs at short intermolecular distance $d=2.8$ Å in Ne complex. This is a contribution from the Schumann–Runge system and from the $a^1\Delta_g-{}^1\Delta_u$ transitions. At long intermolecular distance $d=3.8$ Å the comparison indicates that the D^z_{a-X} transition moment in Ne complex is 9×10^{-6} ea_0 higher than in He complex which corresponds to 22% increase.

The ratio of the Einstein coefficients for the collision-induced $a\rightarrow X$ emission in Ne and He collision complexes, A_{Ne}/A_{He}, is about 1.5 and increases with intermolecular distance from 1.42 at $d=2.8$ Å to 1.79 at $d=3.8$ Å. The equilibrium value for the Ne complex, $d_e=3.87$ Å, is much higher than for the He complex (3.26 Å) in this aug-cc-pVDZ basis set MCSCF calculation. But the difference is not so high in 6-311 G* and 6-311++G(2d,2p) basis sets. In the last method the equilibrium intermolecular distances are equal 3.638, 3.627 and 3.621 Å in the X, a and b states, respectively, in "T-shaped" O_2+Ne complex (oxygen vibration IR transition intensity are equal 0.001 km mol^{-1} for all three states). For O_2+He complex the equilibrium intermolecular distance in low lying states is about 3.26 Å in all basis sets. The repulsive part of the intermolecular potential starts to grow significantly at about 3 and 3.3 Å, respectively, in He and Ne complexes. Vibrational average of the D^z_{a-X} transition moment for $v=0$ intermolecular vibration produces comparable Einstein coefficient for both complexes accounting results of Tables 5 and 2. Unfortunately we can not calculate the realistic PES and the $a-X$ transition moment with high accuracy simultaneously in order to predict the collision-induced $a\rightarrow X$ emission in Ne and He collision complexes. At this point we can conclude that the comparison of Tables 5 and 2 seems to be in qualitative agreement with available experimental data [1–3].

In addition to this comparison between He and Ne complexes we want to illustrate applicability of different computational schemes taken the O_2+Ne complex as an example.

In Table 6 the QR results for the $a-X$ transition intensity calculations in different basis sets are presented. The largest basis set, cc-pVQZ (165 AO's), gives almost the same result as the aug-cc-pVDZ (69 AO's); a very weak D^y component is getting stronger in larger basis sets, Table 6. Increase of polarization functions also leads to some enhancement of the collision-induced $a\rightarrow X$ emission. These results indicate that the basis set superposition error in such extensive basis sets is not of principal importance in the QR calculations of the singlet–triplet transition intensity as has been shown before [76].

Much more important is a qualitatively correct choice of the CAS in MCSCF part. In Fig. 3 the QR results for the $a-X$ transition intensity calculations in smaller CAS are presented. In this CAS the $1\pi_{u,z}$–MO has not been included (all others—$3\sigma_{g,u}$ $1\pi_g$ and $2\pi_u$ orbitals-are included). As a result the $a^1\Delta_g$ state of the $^1A_1$ symmetry has been obtained almost in the closed shell form. In this case the $a-X$ transition of oxygen molecule

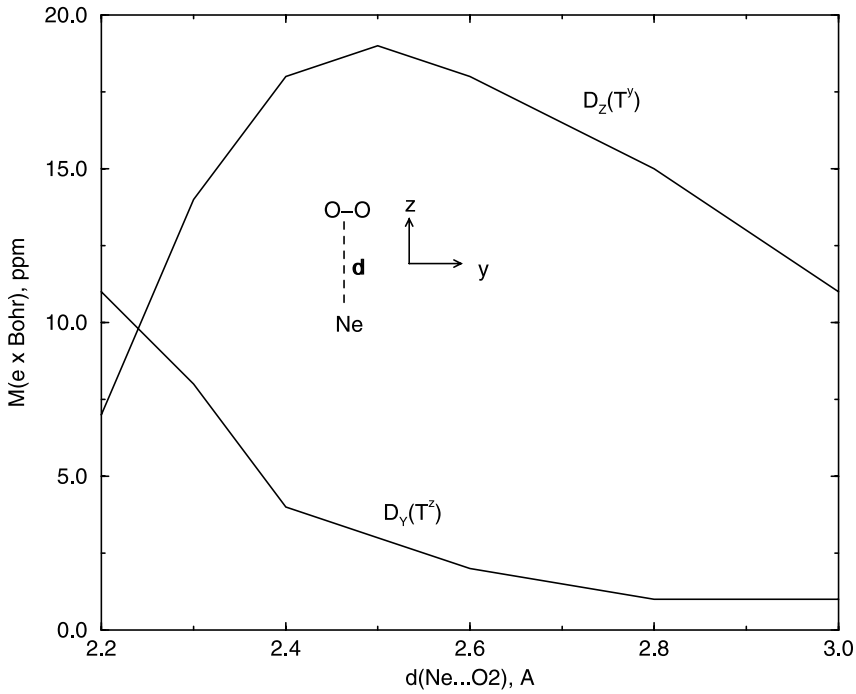

Fig. 3. Collision-induced $a-X$ transition dipole moments in O_2+Ne complex calculated by MCSCF QR method in small CAS (see text) with the 6-31G basis set.

demonstrate a blue shift in collision with Ne atom. The $a-X$ transition moment along the intermolecular z axis $D^z_{a-X}(T^y)$ is weaker than in a proper CAS-I calculations (Table 5, but the $D^y_{a-X}(T^z)$ transition moment along the intramolecular y axis is stronger and increases at a very short contact. These results demonstrate the importance of a proper CAS choice. We should note that a wrong convergence to the closed shell form of the $a^1\Delta_g$ state have been obtained even in CAS-I at short distances; the results also depend on the basis set chosen. In these cases a very strong enhancement of the $a-X$ transition moment resulted, which has no physical meaning (Figs. 3–6).

MCSCF calculations of quadrupole moments in O_2+X complexes, where X = He, Ne, are presented in Table 12. The same geometry of the complexes has been used: $r_{O-O} = 1.207$ Å, $d = 3.2$ Å. The respective quadrupole tensor of the O_2 molecule in the same CAS in the $a^1\Delta_g$ state is equal to: $Q_{yy} = -0.114$ e Å^2; $Q_{xx} = Q_{zz} = 0.057$ e Å^2. Comparison with Table 12 indicates that the absolute value of the parallel component Q_{yy} increases upon complexation in the $a^1\Delta_g$ state, as well as the intermolecular component Q_{zz}. The increase is higher in the Ne atom complex than in the He one.

Similar results have been obtained for the optimized geometries of all species. The asymmetry in quadrupole moment induced by intermolecular interaction is higher for the stronger binding between O_2 and rare gas atom. There is a good correlation between increase of the parallel component Q_{yy} and a rise of the dissociation energy of the complex. Such correlation has been found earlier for the O_2+O_2 dimer [36]. The quadrupole moment of O_2 molecule induces a dipole moment of the rare gas atom. The latter dipole moment produces further deformation of oxygen electronic cloud and finally the asymmetry in the total quadrupole moment of the complex occurs.

The dipole moment of the O_2+Ne complex is much higher that that of the O_2+He one. The dipole moments do not correlate with the energy

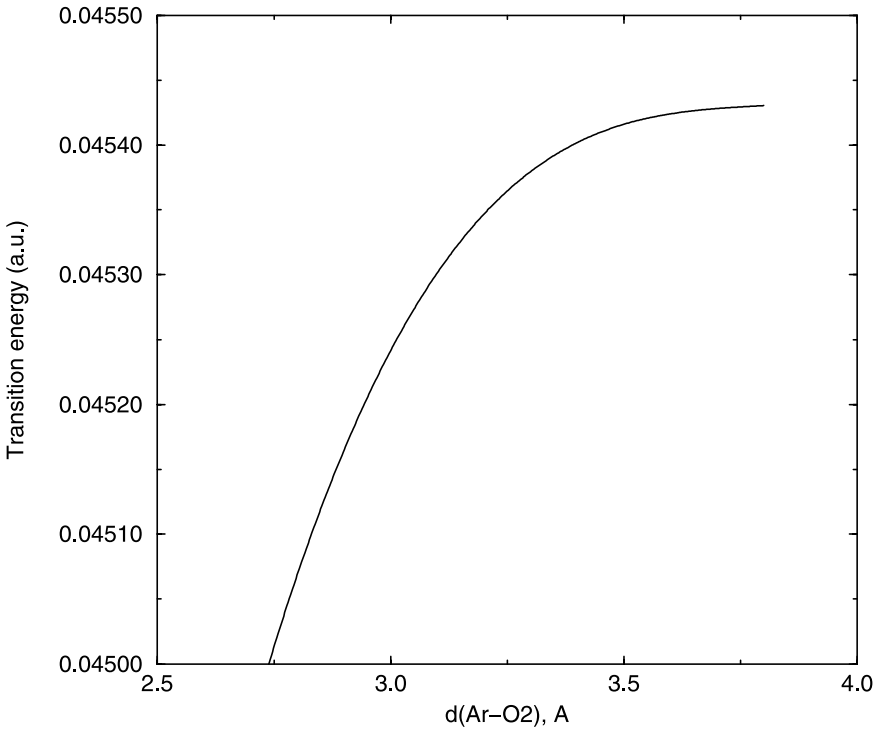

Fig. 4. The calculated red shift of the $a-X$ transition frequency in O_2+Ar collision complex in $2p(O_2)-CAS$ with the 6-31G basis set.

of the complex formation. Ogilby [18] have studied recently the $a-X$ transition energy shift in a number of solvents using the semicontinum model proposed before for the $C_6H_6+O_2$ system [33]. The collision complex $C_6H_6+O_2$ is surrounded by the "solvation shell" and the rest of the solvent volume is simulated by the dielectric continuum model. The solvent is treated as a homogeneous dielectric medium that surrounds a spherical cavity containing the $C_6H_6+O_2$ complex. The medium with dielectric constant ξ produces a reaction field with a self-consistent coupling to the electric charges of the complex. The multipole expansion includes dipolar, quadrupolar and higher terms until $l=10$ [33]. Such a model reproduces pretty well the $a-X$ transition energy red shift in a number of solvents [18]. It has been shown that the energy shift depends principally on the quadrupolar and higher order coupling terms between the complex and the outer solvent and only minimally on the dipolar coupling term [18]. Our results on stabilization energies of the a and X states in the collision complexes with rare gas atoms obtained by MCSCF calculations also illustrate the same trend.

The polarizability of the rare gas atom determines the deformation of the quadrupole moment of the complex. In liquid solvents the polarizability correlates with ξ value. The long-range electrostatic interaction with solvent represents this deformation and this is the reason why the quadrupolar coupling term is so important in stabilization energies of the a and X states.

At the same time the semicontinuum model of "solvation shell" for the van-der Waals complex does not change results of the QR calculation of the $a-X$ transition probability in a free complex itself. The short-range interactions, which depend on orbital overlap and polarizability of the perturber, are important in orbital mixture of the

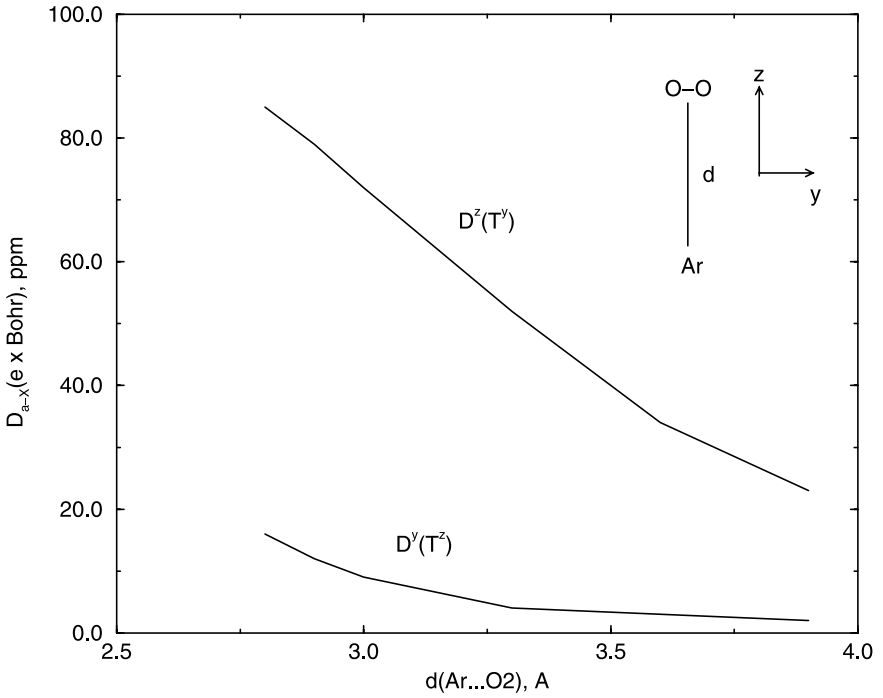

Fig. 5. Collision-induced $a-X$ transition dipole moments in O_2+Ar complex calculated by MCSCF QR method in $2p(O_2)-CAS$ with the 6-31G basis set.

type, given in Eq. (12). This finally determines the $a-b$ transition enhancement and hence, the $a-X$ transition rate.

3.4. O_2+Ar collisions

For O_2+Ar complex the MCSCF convergence to the proper biradical-type wave function, Eq. (2), has been obtained only in 6-311G* and smaller basis sets (Table 7).

The calculated $a-X$ transition dipole moment is much stronger than that for He and Ne collisions. Though the equilibrium has been found at $d \sim 3.9$ Å, a very flat potential stretchs until 3.6 Å, where repulsion starts to grow. At this easily achieved distance the collision induced $a-X$,0 transition dipole moment has a value of 2.5×10^{-5} ea_0 (Table 7), which is much higher than 1.1×10^{-5} ea_0 and 0.9×10^{-5} ea_0 at the same distance in collision complexes with Ne and He, respectively. The calculated lifetime at a short contact ($\tau_R = 66$ s) is in excellent agreement with the Ar matrix isolation measurement, $\tau_R = 68\pm2$ [12] (Tables 7 and 8).

The results of the MCSCF geometry optimization for the O_2+Ar complex of the C_{2v} symmetry are presented in Table 11. The intermolecular distance d is very close to 4 Å in all tree lower states of oxygen moiety. It is getting slightly shorter going from the ground X^3B_1 state ($d=$ 3.9986 Å) to the a and b states ($d=3.9983$ and 3.9971 Å) respectively. (In Table 11 the O–Ar distances are presented). The O–O distance increases in the same manner like in the free O_2 molecule. Vibrational frequency in the complex corresponds to the oxygen vibration; intermolecular vibrations are not obtained in Hessian diagonalization (they are too low) besides the two upper states. The collision induces a dipole moment of the complex, which is larger in the ground state ($\mu=0.006$ D), than in the singlet a and b states (0.005 and 0.0046 D, respectively). The dipole moment has a minus sign, which corresponds to a charge transfer $O_2^-Ar^+$ in the $a^1\Delta_g$ and $b^1\Sigma_g^+$ states [77,78]. A nonzero derivative of

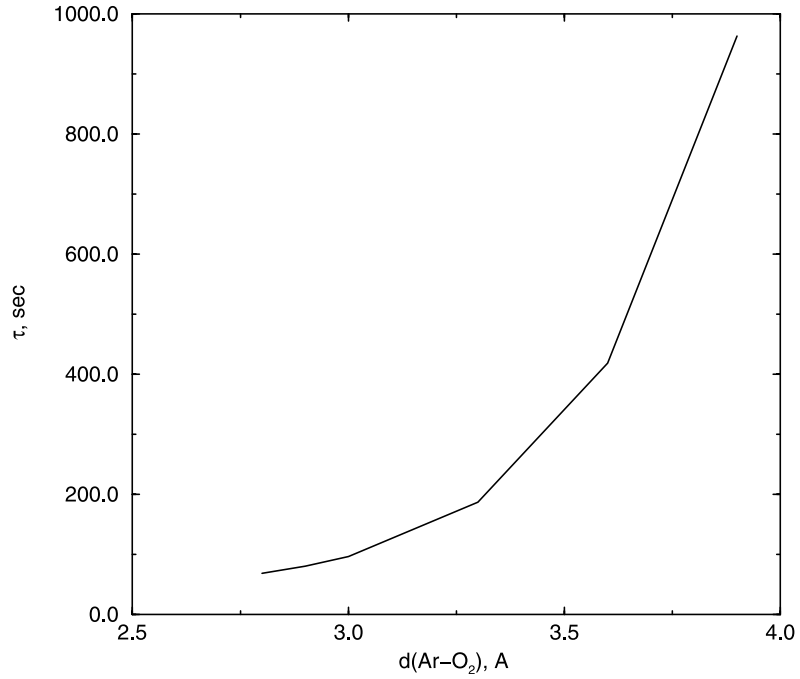

Fig. 6. Radiative lifetime of the $a^1\Delta_g$ state in O_2+Ar complex calculated by MCSCF QR method in $2p(O_2)-$CAS with the 6-31G basis set.

the collision-induced dipole moment along O–O vibrational movement is obtained for all states; the corresponding IRI is presented in Table 11. In the contrast to the linear complex O_2+He, Table 9, the IRI is higher in the ground state; it is equal 0.004 km mol^{-1}, or 0.0001 (D Å^{-1})^2 amu^{-1} (amu is the atomic mass unit). The collision-induced IR absorption of $O_2(a^1\Delta_g)$ near 1500 cm^{-1} should has smaller probability (Table 11) than the ground state IR absorption. The MCSCF geometry optimization in CAS-I for the O_2+Ar complex in the upper states, c, A' and B reveals much stronger intermolecular interaction (Table 11). For example, in the $B^3\Sigma_u^-$ state of oxygen (2^3A_2 state of the complex) the intermolecular distance is shorter and intermolecular vibrations are easily obtained by Hessian diagonalization. One can see from the footnote of the Table 11 that the symmetric intermolecular vibration of the a_1 symmetry (ω_2) has comparatively large probability (IRI $\sim$ 0.005

Table 7
QR calculations of the $a^1\Delta_g \rightarrow X^3\Sigma_g^-$ transition intensity, obtained at different intermolecular distances for the C_{2v} geometry of the O_2+Ar collision; D (ea_0) is electric dipole $a-X$ transition moment, d is intermolecular distance, τ_R is a radiative lifetime of the $a^1\Delta_g(1^1A_1)$ state, A^z is the Einstein coefficient for spontaneous emission polarized along z axis. CAS-I, 6-311G* basis set, $r_{O-O} = 1.207$ Å

d (Å)	$D^z_{a-X}(T^y)$ (ea_0)	$D^y_{a-X}(T^z)$ (ea_0)	ΔE_{a-X} (a.u.)	τ_R (s)	A^z_{a-X} (s^{-1})	A^y_{a-X} (s^{-1})	E($a^1\Delta_g$) (a.u.)
2.8	0.000076	0.000007	0.049358	65.9	1.49×10^{-2}	1.21×10^{-4}	−676.541989
3.0	0.000056	0.000004	0.04944	123.3	8.02×10^{-3}	0.50×10^{-4}	−676.545422
3.2	0.000042	0.000003	0.04949	217.5	4.52×10^{-3}	2.29×10^{-5}	−676.547027
3.4	0.000032	0.000003	0.049513	369.7	2.71×10^{-3}	1.03×10^{-5}	−676.547752
3.6	0.000025	0.000002	0.049522	616.4	1.61×10^{-3}	0.71×10^{-5}	−676.548063

Table 8
QR calculations of the $b^1\Sigma_g^+ \rightarrow X^3\Sigma_g^-$ transition intensity, induced by the O_2+Ar collision. D (ea_0) is electric dipole $b-X$ transition moment, obtained at different intermolecular distances for the C_{2v} geometry of collision; d is intermolecular distance, τ_R is a radiative lifetime of the $b^1\Sigma_g^+$ state, A^z is the Einstein coefficient for spontaneous emission polarized along z axis. CAS-I, 6-311G* basis set, $r_{O-O} = 1.207$ Å

d (Å)	$D^z_{b-X}(T^y)$	$D^y_{b-X}(T^z)$	ΔE_{b-X} (a.u.)	τ_R (s)	A^z_{b-X} (s^{-1})	A^y_{b-X} (s^{-1})	E($b^1\Sigma_g^+$) (a.u.)
3.0	0.000019	0.000016	0.070296	216.3	2.67×10^{-3}	1.90×10^{-3}	−676.411370
3.2	0.000017	0.000011	0.070372	315.8	2.18×10^{-3}	0.98×10^{-3}	−676.517306
3.4	0.000014	0.000009	0.070411	473.4	1.55×10^{-3}	0.55×10^{-3}	−676.518011
3.6	0.000011	0.000007	0.070428	777	0.93×10^{-3}	0.35×10^{-3}	−676.518313
3.8	0.000008	0.000006	0.070431	1405	0.47×10^{-3}	0.24×10^{-3}	−676.518427
4.0	0.000005	0.000005	0.070427	2630	0.21×10^{-3}	0.17×10^{-3}	−676.518457

km mol^{-1}) in the last two upper states. The ω_2 vibration includes a large amplitude movement of all atoms (0.1317 Å shift of both oxygens and −0.1055 Å shift of Ar atom along z intermolecular axis). The large intensity of the ω_2 vibration is explained by large charge transfer admixtures to the $A'^3\Delta_u(1^3B_2)$ and $B^3\Sigma_u^-(2^3A_2)$ states of the complex. The charge transfer state energy strongly depends on intermolecular distance and mixing with this state produces large derivative of the collision-induced dipole moment of the $B^3\Sigma_u^-$ term along the intermolecular movement. The ω_3 vibration is a pendulum movement (mostly of oxygen atoms) around y (oxygen) axis in the yz plane. This intermolecular vibration has small transition moment and is inactive in the IR spectrum of the $A'^3\Delta_u$ state (1^3B_2). It is interesting that in the other $A'^3\Delta_u$ state component (1^3A_2) the oxygen vibration band at 717 cm^{-1} has larger probability (IRI = 0.047 km mol^{-1}) than all other collision-induced infrared transitions. The dipole moment of this state (0.012 D) is not so high like in the 1^3B_2 state (0.023 D), but its derivative in respect to the O–O intramolecular vibration is extremely large. Together with the intrinsic IR transition $c-A$ in a free oxygen molecule at 2400 cm^{-1} predicted as a magnetic dipole radiation [79], the strong collision induced infrared transitions from the metastable states of oxygen predicted in this work (Tables 9 and 11) could be used for atmospheric studies. We have found that the Schumann–Runge transition $X^3\Sigma_g^- - B^3\Sigma_u^-$ intensity diminishes upon collision. For example, in O_2+He collision complex the $X-B$ ($1^3B_1-2^3A_2$) transition moment decreases from 0.895 ea_0 at $d = 3.6$ Å to 0.887 ea_0 at $d = 3$ Å. Much stronger decrease has been obtained before for $O_2+C_6H_6$ [33] and $O_2+C_2H_4$ complexes [59]. The decrease of the Schumann–Runge transition intensity upon collisions can be explained by intensity borrowing to other bands [59]. One of these bands is connected with the Herzberg III transition $X^3\Sigma_g^- - A'^3\Delta_u$ [59,33]. In O_2+X com-

Table 9
MCSCF geometry optimization of the linear O_2+He complex in different states and the collision-induced infrared activity; CAS-I, aug-cc-pVDZ basis set, ω_1 is the O–O vibrational frequency, cm^{-1}, IRI is infrared absorption intensity, km mol^{-1}

Ψ_n	r_{O-O} (Å)	r_{O-He} (Å)	ω_1	IRI	μ (Debye)	E_n (a.u.)
$X^3\Sigma_g^-(1^3A_2)$	1.226	3.989	1548.0	0.000	0.00145	−152.627059
$a^1\Delta_g(1^1A_1)$	1.238	3.985	1457.8	0.008	0.01406	−152.584776
$b^1\Sigma_g^+(2^1A_1)$	1.251	3.980	1370.4	0.000	0.00139	−152.558752
$c^1\Sigma_u^+(1^1A_2)$	1.546	3.882	722.4	0.002	−0.01344	−152.471493
$A'^3\Delta_u(1^3A_1)$	1.548	3.881	714.2	0.011	−0.00964	−152.471665
$A^3\Sigma_u^+(2^3A_2)$	1.537	3.885	774.0	0.000	0.00152	−152.470581
$B^3\Sigma_u^-(3^3A_2)$	1.624	3.856	709.7	0.001	0.00284	−152.391324
$1^5\Pi_g(1^5B_2)$	3.300	3.404	56.5	0.028	−0.08549	−152.460953

plex the $X^3\Sigma_g^- - A'^3\Delta_u$ transition ($1^3B_1 - 1^3A_2$) has an electric dipole transition moment like the Schumann–Runge band ($1^3B_1 - 2^3A_2$) does; both are allowed by symmetry with polarization along intramolecular y axis. In O_2+He complex the $X - A'$ transition moment increases from 0.0005 ea_0 at $d = 3.6$ Å to 0.0014 ea_0 at $d = 3$ Å. In O_2+Ar complex the increase is much higher: from 0.0007 to 0.0162 ea_0 at the same distances, respectively. Transition to the other component of the $A'^3\Delta_u$ state ($1^3B_1 - 1^3B_2$) is forbidden by symmetry. Thus the enhancement of the $X^3\Sigma_g^- - A'^3\Delta_u$ band (high pressure band) by collisions with inert gases is not so strong like in O_2+C_6H_6 collisions [33]; it strongly depends on ionization potential of collider and determined by charge transfer mixing of the $A'^3\Delta_u$ and $B^3\Sigma_u^-$ states [33,59]. LR calculation of the SOC integral, Eq. (8), with the $b^1\Sigma_g^+(2^1A_1)$ state of the O_2+Ar complex as the MCSCF reference state in 6-311G* basis with CAS-II produces 174.766 cm^{-1} at $d = 3.6$ Å and 174.718 cm^{-1} at $d = 3.2$ Å. (174.792 cm^{-1} is obtained at the dissociation limit). At the same time the SOC integral $\langle a^1\Delta_g(1^1A_1)|H_{so}|X^3\Sigma_g(^3B_1)\rangle$ is getting nonzero and is equal 0.335 cm^{-1} at $d = 3.6$ Å and 0.955 cm^{-1} at $d = 3.2$ Å. Similar results have been obtained before in MNDO/3 CI study of O_2+C_2H_4 complex [38,40] This contributes to the $a - X,0$ transition moment by the difference of the permanent dipole moments of the a and X states. Since the difference is not large (10^{-4} D), this contribution is negligible. The 6-31G basis set calculations for Ar+O_2 complex produce reasonable results; there is a red shift of the $a - X$ frequency and the collision induced $a - X,0$ transition dipole moment has a value of about 2×10^{-5} ea_0 at $d = 3.6$ Å (easily achieved distance). The O–O distance was fixed at $r_{O-O} = 1.22$ Å. Similar calculations with the 6-311G basis set for Ar+O_2 complex produce unreasonable blue shift (very small) and slightly smaller collision induced $a - X,0$ transition dipole moment. Finally the 6-311G* basis set was found the most reliable for the Ar+O_2 complex calculations with CAS-I active space Table 7.

The aug-cc-pVDZ basis set for Ar+O_2 complex produces the closed shell structure of the a state at all intermolecular distances and these results are physically unreasonable, since a strong SOC mixing between the a and $X,0$ states occurs ($\langle H_{so}\rangle = 106$ cm^{-1}).

3.5. Configuration interaction calculations

All complexes have been calculated by restricted open shell Hartree–Fock method (ROHF) in the ground triplet state with subsequent configuration interaction (CI) calculations for spin-allowed singlet–singlet (S–S) and triplet–triplet (T–T) transitions without symmetry restrictions (C_1 point group) by GAMESS code. SOC matrix elements have also been calculated. Such simple approach permits to get a new insight by comparison with the MCSCF response method. Since these CI calculations have only an auxiliary and qualitative meaning a small 6-31G basis set has been used.

The ''T-shaped'' complex with He atom at $d = 3.2$ Å demonstrate the following interesting feature. The $2\sigma_u$ and He orbitals have almost the same energy ~ -0.92 a.u. The $3\sigma_g$, $1\pi_u$ and $1\pi_g$–MO's energies are -0.654, -0.474 and -0.229 a.u., respectively. The empty orbitals are characterized by a big gap between the lowest $3\sigma_u$ (0.387 a.u.) and the next, $2\pi_u$ (0.968 and 0.971 a.u.), MO's (MO energy is in brackets). Them follow high density of orbitals: $4\sigma_u$ (1.068 a.u.), $2\pi_g$ (1.089 a.u.) and $4\sigma_g$–MO's (1.094 a.u.). All these orbitals have been taken into account in the CI calculations. Transitions between ten lowest excited states of each multiplicity have been studied. The most intensive T–T transitions are the Schumann–Runge (0.877 ea_0) and the $1^3\Pi_g - 2^3\Pi_u$ (0.920 ea_0) transitions, with vertical excitation energies at $r = 1.207$ Å equal 9.6 and 7.6 eV, respectively. We should remind that the $1^3\Pi_g$ state has a very shallow minimum because of avoided crossing [79]; near the minimum at $r = 1.55$ Å the $1^3\Pi_g - 2^3\Pi_u$ transition energy is lower, 5.8 eV. Recently predicted $A'^3\Delta_u \rightarrow 1^3\Pi_g$ absorption band with transition moment 0.136 ea_0 [79] is enhanced by collision with He atom; at $r = 1.207$ Å the transition moments are in the range 0.213–0.221 ea_0 for four allowed components (transition energies are equal 2.36 eV, oscillator strengths are about 0.04). The most intensive S–S transition,

$a^1\Delta_g(^1B_1)$–$1^1\Delta_u(^1B_2)$ (0.742 ea_0) has a vertical excitation energy 11 eV.

The collision-induced a–b transition is weaker in CI calculation. At $d = 3.2$ Å the 1^1A_1–2^1A_1 transition moment is 0.00027 ea_0, the other component of the $a^1\Delta_g$ state, 1^1B_1, has the a–b transition moment equal 0.00004 ea_0.

Transitions to the $1^1\Pi_g$ state are the most intensive collision-induced S–S bands. The $a^1\Delta_g(1^1A_1)$–$1^1\Pi_g(^1B_2)$ transition moment is 0.00048 ea_0 and polarized along the O–O axis (y); almost the same intensity has the $a^1\Delta_g$–$1^1\Pi_g$ transition between other components (1^1B_1–$^1A_2$). Similar transition from the $b^1\Sigma_g^+$ state (2^1A_1–$^1B_2$) is less intensive (0.00014 ea_0). The MCSCF LR calculations produce much stronger intensity (Table 1). Transition moments to the $1^1\Pi_u$ states from the a (0.122 ea_0) and b terms (0.114 ea_0) are also smaller than in MCSCF LR method (Table 1).

Absorption from the $c^1\Sigma_u^-$ state to the both $1^1\Pi_g$ sublevels ($D^{x,z} = 0.218$ ea_0) is very similar to the $A'^3\Delta_u \rightarrow 1^3\Pi_g$ absorption bands, but is less sensitive to collisions.

The highest SOC matrix element induced by collision with He atom at $d = 3.2$ Å was found to be $\langle c^1\Sigma_u^- | H_{so}^y | A'^3\Delta_u \rangle = 4.2$ cm^{-1}. All other SOC integrals induced by collision have an order 0.1–0.01 cm^{-1}.

We should stress a new and unexpected result: the $^1\Pi$ states are splitted by collisions with He atom and transitions between two components are getting electric dipole allowed. For example, the $1^1\Pi_g$ state splits by 19 cm^{-1} and transition moment is 0.00007 ea_0. For the $1^1\Pi_u$ state the splitting is 21 cm^{-1}; the transition moment is smaller (0.00002 ea_0). Much stronger intensity predicted for the triplet $^3\Pi$ states; in these states the collision-induced splitting of the same order should be added to the SOC splitting, which is much higher ($A_{so} = 72$ cm^{-1} for the $1^3\Pi_g$ term). The collision-induced transition moment between two orbital components of the $^3\Pi_g$ state is $D^x =$ 0.00024 ea_0; the dipole velocity is $3.3 \times 10^{-5} \frac{e}{a_0}$, which gives the oscillator strength equals 9×10^{-6}. With SOC account this will lead to comparatively strong transitions between $^3\Pi_0$ and $^3\Pi_2$ components separated by about 200 cm^{-1}.

Splitting of the $a^1\Delta_g$ state in O_2+He complex at $d = 3.2$ Å is negligible (0.05 cm^{-1}). But in O_2+Ne complex it is higher (2.3 cm^{-1}) and increases till 7.6 cm^{-1} at $d = 3$ Å.

Finally, the most intensive collision-induced transition is predicted for the $1^3\Pi_g$–$1^3\Pi_u$ forbidden band with energy 1.89 eV. The collision-induced electric dipole transition moment is 0.025 ea_0; the dipole velocity is $0.031 \frac{e}{a_0}$, which gives the oscillator strength equals 0.009. The latter value is higher than the oscillator strength obtained with the dipole moment approximation, but a qualitative conclusion about possible observation of the collision-induced $1^3\Pi_g$–$1^3\Pi_u$ transition seems to be quite definite.

3.6. IR absorption of the $O_2(^5\Pi_g)$ state induced by collision with He the third particle

Our calculations indicate that the most interesting collision-induced IR intensity occurs in the metastable quintet states of the two oxygen atoms radical pair, two O(^3P). The van der Waals state of the oxygen atoms pair, $^5\Pi_g$, can bind the third particle, for example He; a low frequency IR transition connected with the O–O vibration of the $^5\Pi_g$ state is strongly enhanced in such a complex (consider the last row of Table 9).

The $^5\Pi_g$ state has a predicted O–O vibration frequency in the range 113–237 cm^{-1} and dissociation energy, 0.1–0.16 eV, as it follows from the most accurate ab initio results [75]. Recombination of two O(^3P) atoms produces an excited O_2 * precursor; in order to relax to the b and a states it should transfer energy to the third particle. It was suggested that 70% of all associations initially populate the $^5\Pi_g$ state at 200 K [80]; latter the importance of this state has been reduced [75]. When the $^5\Pi_g$ state is formed by recombination of two O(^3P) atoms on the surface of small aerosle particle the release of small energy (0.16 eV) can easily by accepted by the particle. If the recombination leads to the tightly bound states of O_2 molecule the release of high energy (1–5 eV) would

Table 10
MCSCF geometry optimization of the T-shaped O_2+He complex in different states and the collision-induced infrared activity; CAS-I, aug-cc-pVDZ basis set, vibrational frequencies ω_i are in cm^{-1}

Ψ_n	r_{O-O} (Å)	r_{O-He} (Å)	ω_1	ω_2[a]	ω_3[a]	μ (Debye)	E_n (a.u.)
$X^3\Sigma_g^-(1^3B_1)$	1.226	3.256	1548.4	64.0	25.9	0.00041	−152.627005
$a^1\Delta_g(1^1A_1)$	1.238	3.257	1454.5	62.7	27.3	0.00024	−152.584204
$b^1\Sigma_g^+(2^1A_1)$	1.251	3.257	1370.7	61.8	27.7	0.00027	−152.558760
$A'^3\Delta_u(1^3B_2)$	1.539	3.261	767.2	47.2	23.2	0.00886	−152.470698
$A'^3\Delta_u(1^3A_2)$	1.537	3.260	774.4	58.5	28.7	0.00117	−152.470534
$A^3\Sigma_u^+(2^3B_2)$	1.545	3.260	756.0	58.4	28.6	0.00184	−152.467246

[a] In all states the intermolecular vibrations ω_2 of a_1 symmetry and ω_3 of b_2 symmetry have been obtained; IRI = 0 for all IR transitions. The only exception concerns the $A'^3\Delta_u(1^3B_2)$ state, where IRI(ω_1) = 0.001 and IRI(ω_2) = 0.004.

lead to dissociation of the aerosle particle. Thus the $^5\Pi_g$ state of the $O_{2\,*}$ precursor adsorbed on the aerosle particles would be inreached, since other particles disappear. The important sequence of our model is that infrared absorption of adsorbed $O_{2\,*}(^5\Pi_g)$ molecules in the range 56–237 cm^{-1} can be detected.

3.7. Cooperative phenomena

Calculations of triple complexes O_2+2M have been performed with many different mutial orientations. The symmetric rhombus configuration of the D_{2h} point group, as well as symmetric linear structure do not produce enhancement of the a–X and a–b transitions. The nature of the electric dipole a–b transition moment is determined by intermolecular polarization and charge transfer; both are vector properties. Thus the a–b transition moments induced by perturbers from opposite sides cancel each other [38,58]. All asymmetric structures are quite efficient in the a–X and a–b transitions enhancement. A simple additive vector model (when the a–b transition moment vectors induced by each partner are summarized) does not coincide exactly with the triple complex calculation. Deviation depends on mutial orientations. The simplest way to describe this cooperative effect is presented by helium clusters O_2+He_n calculations. In one model a linear He_3 cluster was situated parallel to O–O axis. The distance between two parallel axes, d = 2.6 Å, and the middle He atom is just under the center of the O–O bonds (like in Fig. 1b, without the fourth He atom). This He–O distance is 2.67 Å, the terminal He–O distances are 3.1 Å; r(He–He) = 2.3 Å. The middle, nearest, He atom produces the largest perturbation; in O_2+He complex the a–b transition moment is 0.006 ea_0 (Table 3) and the a–X transition moment equals $D^z_{a-X}(T^y) = 0.000028$ ea_0 (Table 2). Interaction with He_3 cluster produces $D^z_{a-b} = 0.0072$ ea_0 and $D^z_{a-X}(T^y) = 0.000033$ ea_0. The radiative lifetime drops from 393 s (Table 2) to 266 s. The a–X transition energy is blue shifted to 0.053874 a.u.

When the fourth He atom was situated below the middle one by the same r(He–He) = 2.3 Å distance (Fig. 2b), the following results of the LR and QR calculations have been obtained: $D^z_{a-b} = 0.0079$ ea_0 and $D^z_{a-X}(T^y) = 0.000037$ ea_0. The a–X transition energy is almost non changed (0.053875 a.u.). The radiative lifetime drops further to 220 s. The same CAS has been used in all these MCSCF calculations. Further increase of next neighbors leads to a fast saturation of the effect. The plane cluster He_8 gives the $O_2(a^1\Delta_g)$ radiative lifetime of 204 s. Interaction with bulky cluster produces similar effects from the nearest and further neighbors. More details are published somewhere [81].

4. Conclusions

Geometry optimizations of different states of the complexes O_2+X, where X = He, Ne, Ar,

illustrate how an infrared absorption of oxygen molecule is induced by collisions. Intensity of this infrared absorption depends on polarizability of collider. Similar calculations for O_2 collisions with Li_2 molecule, which possesses the largest polarizability produces the IR intensity, which achieves 0.1 km mol^{-1} (compare with Tables 9–11).

The strongest collision-induced IR intensity occurs in the metastable quintet state, $^5\Pi_g$, of the two oxygen atoms radical pair, two O(^3P). This weakly bound van der Waals state of the oxygen atoms pair has not been observed so far and our calculations propose a way of its experimental observation.

The important results from the linear O_2+He complex geometry optimizations is that the intermolecular distances r_{O-He} are shorter for the higher excited states. Quite similar trends have been obtained in a previous calculations of other complexes [58,34]. More tightly bound excited states have been obtained for other complexes studied in present work (O_2+Ar, O_2+Li_2). The result seems to be quite general.

All rare-gas collision-induced transition dipole moments are practically negligible at large distances, $d \geq 5$ Å, and grows appreciable only at $d \simeq d_e$. The $b-a$ transition moment is larger than the moments for other low-energy collision-induced transitions, like the $a^1\Delta_g(^1B_1)$–$c^1\Sigma_u(^1A_2)$ band (only UV transitions to the Π_g states are stronger enhanced). In O_2+He complex the D^y_{a-c} electric-dipole transition moment is twice as small as the D^y_{a-b} at $d = 3.6$ Å.

It was pointed out previously [34] that the $b-X$, 0 transition can acquire the collision-induced electric dipole transition moment through the difference of the electric dipole moments of the X and b states. In the O_2+He collision complex at $d = 3.2$ Å and $r_e = 1.23$ Å, this difference is about 0.0002 Debye (Table 10). The QR calculated $D^z_{b-X}(T^y)$ transition moment nearly corresponds to this mechanism (Table 4). But the transition to the $M_S = 1$ component $b-X$, 1 is also induced and is stronger: $D^y_{b-X}(T^z) = 0.000007\ ea_0$ at $d = 3.2$ Å (Table 4). It is only twice as small as the $a-X$ transition moment (Table 2). The $b-X$, 1 transition borrows intensity from the Schumann–Runge system because of nonzero SOC (Table 1). Still the collision-induced $b-X$ transition enhancement is negligible in comparison with the intrinsic magnetic-dipole probability $A_{b-X} = 0.087$ s^{-1} [62].

The $a-X$ transition is greatly enhanced in solvents by borrowing intensity from the collision induced $b-a$ transition, as described above. In contrast, the $b-X$ transition, being comparatively intensive in free molecules, lacks an effective source for intensity borrowing upon collision [38,65], so its radiative probability is not much enhanced in condensed media.

Table 11
MCSCF geometry optimization of the T-shaped O_2+Ar complex in different states and the collision-induced infrared activity; CAS-I, 6-311G* basis set, ω is the O–O vibrational frequency, cm^{-1}; IRI is the infrared intensity, km mol^{-1}

Ψ_n	r_{O-O} (Å)	r_{O-Ar} (Å)	ω	IRI	μ (Debye)	E_n (a.u.)
$X^3\Sigma_g^-(1^3B_1)$	1.220	4.045	1563.7	0.004	−0.00609	−676.588487
$a^1\Delta_g(1^1A_1)$	1.232	4.045	1476.8	0.003	−0.00512	−676.548992
$b^1\Sigma_g^+(2^1A_1)$	1.248	4.045	1373.9	0.002	−0.00465	−676.520364
$c^1\Sigma_u^-(1^1A_2)$	1.537	3.948	723.6	0.002	−0.00623	−676.433248
$A'^3\Delta_u(1^3A_2)$	1.538	4.017	717.4	0.047	−0.01234	−676.433258
$A'^3\Delta_u(1^3B_2)$	1.563	3.993	624.3[a]	0.003	−0.02329	−676.423612
$B^3\Sigma_u^-(2^3A_2)$	1.664	3.892	553.7[b]	0.000	−0.01891	−676.347212

[a] In $A'^3\Delta_u(1^3B_2)$ state two intermolecular vibrations have been obtained: a_1, $\omega_2 = 24.12$ cm^{-1}, IRI = 0.005 km mol^{-1} and b_2, $\omega_3 = 21.97$ cm^{-1}, IRI = 0.

[b] In $B^3\Sigma_u^-(2^3A_2)$ state two intermolecular vibrations have been obtained: a_1, $\omega_2 = 28.2$ cm^{-1}, IRI = 0.004 km mol^{-1} and b_2, $\omega_3 = 28.5$ cm^{-1}, IRI = 0.002 km mol^{-1}.

Table 12
MCSCF calculation of the quadrupole moments of the T-shaped O_2+He and O_2+Ne complexes in different states; CAS-I, aug-cc-pVDZ basis set, Q_{xx} is a component of the quadrupole moment, e Å^2; μ is a dipole moment, Debye

Ψ_n	Q_{xx}	Q_{yy}	Q_{zz}	μ	E_n (a.u.)
O_2 +He					
$X^3\Sigma_g^-(1^3B_1)$	0.0125	−0.0274	0.0148	0.00042	−152.626493
$a^1\Delta_g(1^1A_1)$	0.0546	−0.1169	0.0622	0.00035	−152.582997
$b^1\Sigma_g^+(2^1A_1)$	0.0786	−0.1619	0.0833	0.00047	−152.556512
O_2 +Ne					
$X^3\Sigma_g^-(1^3B_1)$	0.012387	−0.027402	0.015015	0.00288	−278.267043
$a^1\Delta_g(1^1A_1)$	0.052211	−0.116962	0.064751	0.00305	−278.223554
$b^1\Sigma_g^+(2^1A_1)$	0.079160	−0.161827	0.082667	0.00332	−278.197072

$r_{O-O} = 1.207$ Å, $d = 3.2$ Å.

Acknowledgements

This work was supported by Wenner-Gren Foundation.

References

[1] T.F. Rajchenok, I.M. Byteva, K.I. Salohiddinov, L.M. Bolotko, Opt. Spectrosc. 49 (1980) 208.
[2] E.H. Fink, K.D. Setzer, J. Wildt, D.A. Ramsay, M. Vervloct, Int. J. Quantum Chem. 39 (1991) 287.
[3] J. Wildt, E.H. Fink, P. Biggs, R.P. Wayne, A.F. Vilesov, Chem. Phys. 159 (1992) 127.
[4] F. Thibault, V. Menoux, R.L. Doucen, Appl. Opt. 36 (1997) 563.
[5] L. Herzberg, G. Herzberg, Astrophys. J. 105 (1947) 353.
[6] B.F. Minaev, Opt. Spectrosc. (USSR) 45 (1978) 936.
[7] B.F. Minaev, Izv. Vyssh. Uchebn. Zaved. Fiz. 9 (1978) 115.
[8] S.P. McGlynn, T. Azumi, M. Kinoshita, Molecular Spectroscopy of the Triplet State, Prentice Hall, Engelwood Cliffs, NJ, 1969.
[9] Z.M. Muldahmetov, B.F. Minaev, G.A. Ketsle. Optical and magnetic properties of the triplet state, Nauka. Alma-Ata (in Russian), 1983.
[10] A.C. Becker, U. Schurath, I.I. Dubost, J.P. Galaup, Chem. Phys. 125 (1988) 321.
[11] R. Böhling, A. Becker, K. Serawski, B.F. Minaev, U. Schurath, Chem. Phys. 142 (1990) 445.
[12] G. Tyczkowski, U. Schurath, M. Bodenbinder, H. Willner, Chem. Phys. 215 (1997) 379.
[13] A.A. Krasnovsky, Jr, Chem. Phys. Lett. 81 (1981) 443.
[14] P.R. Ogilby, C.S. Foote, J. Am. Chem. Soc. 105 (1983) 3423.
[15] A.P. Darmanyan, Khim. Fiz. 6 (1987) 1192.
[16] A.P. Losev, I.M. Byteva, G.P. Gurinovich, Chem. Phys. Lett. 143 (1988) 127.
[17] R.D. Scurlock, S. Nonell, S.E. Braslavsky, P.R. Ogilby, J. Phys. Chem. 99 (1995) 3521.
[18] P.R. Ogilby, Acc. Chem. Res. 32 (1999) 512.
[19] R. Schmidt, E. Afshari, J. Phys. Chem. 94 (1990) 4377.
[20] R. Schmidt, M. Bodesheim, J. Phys. Chem. 98 (1994) 2874.
[21] R. Schmidt, M. Bodesheim, J. Phys. Chem. 99 (1995) 15919.
[22] R. Schmidt, F. Shafii, M. Hild, J. Phys. Chem. A 103 (1999) 2599.
[23] P.K. Frederiksen, M. Jorgensen, P.R. Ogilby, J. Am. Chem. Soc. 123 (2001) 1215.
[24] C.W. Jefford, Chem. Soc. Rev. 22 (1993) 59.
[25] D. Gal. Biochem, Biophys. Res. Commun. 202 (1994) 10.
[26] A.M.D. Batlle, J. Photochem. Photobiol. B20 (1993) 5.
[27] R. Prabhakar, P.E.M. Siegbahn, B. Minaev, H. Ågren, J. Phys. Chem. B 106 (2002) 3742.
[28] H.I. Pass, J. Natl. Cancer Inst. 85 (1993) 443.
[29] A.P. Darmanyan, J. Phys. Chem. A 102 (1998) 9833.
[30] K. Rund, B. Schimmelpfennig, H. Ågren, Chem. Phys. Lett. 310 (1999) 215.
[31] D. Weldon, B. Wang, T.D. Poulsen, P.R. Ogilby, K.V. Mikkelsen, J. Phys. Chem. A 102 (1998) 1498.
[32] J.M. Wessels, M.A.J. Rodgers, J. Phys. Chem. 99 (1995) 17586.
[33] B.F. Minaev, K.V. Mikkelsen, H. Ågren, Chem. Phys. 220 (1997) 79.
[34] B.F. Minaev, H. Ågren, J. Chem. Soc. Faraday Trans. 93 (1997) 2231.
[35] B.F. Minaev, O. Vahtras, H. Ågren, Chem. Phys. 208 (1996) 299.
[36] B.F. Minaev, V.D. Nikolaev, H. Ågren, Spectrosc. Lett. 29 (1996) 677.
[37] B.F. Minaev, Zh. Fiz. Khim. 68 (1994) 1432.
[38] B.F. Minaev, Theoretical analysis and prognostication of spin-orbit coupling effects in molecular spectroscopy and chemical kinetics, Dr. Sc. Thesis, N.N. Semenov Institute of Chemical Physics, Moscow, (in Russian), 1983.

[39] B.F. Minaev, Opt. Spectrosc. (USSR) 58 (1985) 1238.
[40] B.F. Minaev, J. Appl. Spectrosc. (USSR) 42 (1985) 518.
[41] B.F. Minaev, G.K. Mambeterzina, Oxygen complexes with naphthalene and decapenthacne studied by mindo ci method, in: G.A. Ketsle (Ed.), Photoproceses in Atomic, and Molecular Systems (in Russian), Karaganda State University, 1984, p. 35 (in Russian).
[42] B.F. Minaev, S. Lunell, G.I. Kobzev, J. Mol. Struct. (TEOCHEM) 284 (1993) 1.
[43] H. Ågren, O. Vahtras, B.F. Minaev, Adv. Quantum Chem. 27 (1996) 71.
[44] H.J.A. Jensen, P. Jørgensen, T. Helgaker, J. Olsen, Chem. Phys. Lett. 154 (1989) 380.
[45] H. Hettema, H.J.A. Jensen, P. Jørgensen, J. Olsen, J. Chem. Phys. 97 (1992) 1174.
[46] J.S. Binkley, W.J. Hebre, J.A. Pople, J. Am. Chem. Soc. 101 (1980) 939.
[47] D.E. Woon, T.H. Dunning, J. Chem. Phys. 98 (1993) 1358.
[48] W.J. Hebre, R. Ditchfield, J.A. Pople, J. Chem. Phys. 56 (1972) 2257.
[49] S. Koseki, M.H. Schmidt, M.S. Gordon, J. Phys. Chem. 96 (1992) 10678.
[50] M.W. Schmidt, K.K. Baldridge, J.A. Boats, S.T. Elbert, M.S. Gordon, J.H. Jensen, S. Koseki, N. Matsunaga, K.A. Nguyen, S.J. Su, T.L. Windus, J. Comput. Chem. 14 (1993) 1347.
[51] T. Helgaker, H.J.A. Jensen, P. Jørgensen, J. Olsen, K. Ruud, H. Ågren, T. Andersen, K.L. Bak, V. Bakken, O. Christiansen, P. Dahle, E.K. Dalskov, T. Enevoldsen, B. Fernandes, H. Koch, H. Heiberg, H. Hettema, D. Jonsson, S. Kirpekar, R. Kobayashi, K.V. Mikkelsen, P. Norman, M.J. Packer, T. Saue, P.R. Taylor, O. Vahtras, Dalton release 1.0, an Electronic Structure Program, 1997.
[52] B.F. Minaev, J. Mol. Struct. THEOCHEM 183 (1989) 207.
[53] B.F. Minaev, Izv. Vyssh. Uchebn. Zaved. Fiz. 5 (1978) 160.
[54] H. Klotz, C.M. Marian, S.D. Peyerimhoff, B.A. Hess, R.J. Buenker, Chem. Phys. 89 (1984) 223.
[55] O. Vahtras, B.F. Minaev, H. Ågren, Chem. Phys. Lett. 281 (1997) 186.
[56] Y. Luo, D. Jonsson, P. Norman, K. Ruud, H. Ågren, B. Minaev, A. Rizzo, K.V. Mikkelsen, Int. J. Quantum Chem. 70 (1998) 219.
[57] E.B. Sveshnikova, B.F. Minaev, Opt. Spectrosc. 54 (1983) 320.
[58] B.F. Minaev, S. Lunell, G.I. Kobzev, Int. J. Quantum Chem. 50 (1994) 279.
[59] B.F. Minaev, V.V. Kukueva, H. Ågren, J. Chem. Soc. Faraday Trans. 90 (1994) 1479.
[60] R.M. Badger, A.C. Wright, R.F. Whitlock, J. Chem. Phys. 43 (1965) 4345.
[61] J.F. Noxon, Can. J. Phys. 39 (1961) 1110.
[62] K.J. Ritter, T.D. Wilkerson, J. Mol. Spectrosc. 121 (1987) 1.
[63] L.R. Brown, C. Plymate, J. Mol. Spectrosc. 199 (2000) 166.
[64] V.D. Galkin, Opt. Spectrosc. (in Russian) 47 (1979) 266.
[65] B.F. Minaev, Int. J. Quantum Chem. 17 (1980) 367.
[66] R. Klotz, S.D. Peyerimhoff, Mol. Phys. 57 (1986) 573.
[67] P.H. Krupenie, J. Phys. Chem. Ref. Data 1 (1972) 423.
[68] C. Long, D.R. Kearns, J. Chem. Phys. 59 (1973) 5729.
[69] A.A. Krasnovsky, Jr, S.Y. Yegorov, O.V. Nazarova, Y.I. Yartsev, G.V. Ponomarev, Biofizika 32 (1987) 982.
[70] S.E. Gorman, I. Hamblett, C. Lambert, A.L. Prescott, M.A.J. Rodgers, J. Am. Chem. Soc. 109 (1987) 3091.
[71] R.D. Scurlock, P.R. Ogilby, J. Phys. Chem. 91 (1987) 4599.
[72] D. Schroder, H. Schwarz, Angew. Chem. Int. Engl. Ed. 34 (1973) 1995.
[73] M. Hild, R. Schmidt, J. Phys. Chem. A 103 (1999) 6091.
[74] B.F. Minaev, G.I. Kobzev, Opt. Spectrosc. 83 (1997) 58.
[75] H. Partridge, C.W. Bauschlicher, S.R. Langhoff, P.R. Taylor, J. Chem. Phys. 95 (1991) 8292.
[76] B.F. Minaev, S. Knuts, H. Ågren, Chem. Phys. 181 (1994) 15.
[77] B.F. Minaev, Phys. Chem. Chem. Phys. 1 (1999) 3403.
[78] T.D. Poulsen, P.R. Ogilby, K.V. Mikkelsen, J. Phys. Chem. A 102 (1998) 8970.
[79] B.F. Minaev, Chem. Phys. 252 (2000) 25.
[80] D.R. Bates, Chem. Phys. Lett. 162 (1989) 313.
[81] B.F. Minaev, N.M. Ivanova, G.I. Kobzev, Z.M. Muldahmetov, J. Appl. Spectrosc. 29 (2002) 25.